Non-orthogonal Frequency Division Multiplexing with Index Modulation

A Thesis Submitted
to the College of Graduate and Postdoctoral Studies
in Partial Fulfillment of the Requirements
for the Degree of Master of Science
in the Department of Electrical and Computer Engineering
University of Saskatchewan

by

Nghia H. Nguyen

Saskatoon, Saskatchewan, Canada

Permission to Use

In presenting this thesis in partial fulfillment of the requirements for a Postgraduate degree from the University of Saskatchewan, it is agreed that the Libraries of this University may make it freely available for inspection. Permission for copying of this thesis in any manner, in whole or in part, for scholarly purposes may be granted by the professors who supervised this thesis work or, in their absence, by the Head of the Department of Electrical and Computer Engineering or the Dean of the College of Graduate Studies and Research at the University of Saskatchewan. Any copying, publication, or use of this thesis, or parts thereof, for financial gain without the written permission of the author is strictly prohibited. Proper recognition shall be given to the author and to the University of Saskatchewan in any scholarly use which may be made of any material in this thesis.

Request for permission to copy or to make any other use of material in this thesis in whole or in part should be addressed to:

Head of the Department of Electrical and Computer Engineering
57 Campus Drive
University of Saskatchewan
Saskatoon, Saskatchewan, Canada
S7N 5A9
or
Dean
College of Graduate and Postdoctoral Studies
University of Saskatchewan
116 Thorvaldson Building, 110 Science Place
Saskatoon, Saskatchewan Canada,
S7N 5C9

Abstract

Orthogonal Frequency Division Multiplexing (OFDM) is a well-established technique in wireless communications due to its high spectral efficiency compared to other multicarrier schemes. However, the explosion of Internet of Things (IoT) has demanded a more spectrally-efficient technique to utilize small bandwidths, on which numerous low-power low-rate devices operate. This thesis aims to provide solutions for this problem.

First, the integration of index modulation to fast-OFDM, which is a special variant of OFDM, is investigated. The highest obtainable bit rate of this system is derived, which demonstrates enhancements compared to OFDM systems in the low-power low-rate regions. Furthermore, an improved one-dimension constellation is found to optimize the overall bit error rate (BER) of this system. Numerical results show that proposed system exhibits enhancements in both bit rate and error performance, leading to higher spectral efficiency compared to OFDM in the low-power regions.

The second part of the thesis is concerned with reducing the bandwidth consumed by multicarrier transmissions. This results in the mutual orthogonality among subchannels being destroyed, yielding a Non-orthogonal Frequency Division Multiplexing (NFDM) system. The main contribution in this part includes a novel and feasible design for NFDM systems, which is capable of eliminating inter-channel interference (ICI), which is the major limitation of conventional NFDM system. As such, the error performance of proposed system over Gaussian white noise channels is the same as that of an OFDM system. The power spectrum density (PSD) of the proposed system was investigated, leading to design guidelines and tradeoffs between the PSD shape and the system bit rate.

Finally, index modulation is introduced to the proposed NFDM systems. Due to the ICI-free design, this combined system (NFDM-IM) and fast-OFDM-IM share the similar signal detection mechanism. Improved QAM constellations are found for NFDM-IM systems to optimize their overall BER. Obtained results show that with low modulation orders such as 8-QAM, NFDM-IM systems using the improved constellation achieve close error performance to that of NFDM in the low BER regions. With equivalent occupied bandwidth and

error performance, an NFDM-IM system with optimal 8-QAM constellation produces better spectral efficiency than one using the conventional constellation.

Acknowledgments

I would like to express my utmost gratitude to Professor Ha Nguyen and Professor Brian Berscheid for their direct guidance and support in my M.Sc. studies at the University of Saskatchewan. Starting from scratch, I have learned very much on how to conduct a meaningful research thanks to their invaluable criticism and orientations.

I would also like to thank Prof. Eric Salt, Prof. Brian Daku and Mr. Rory Gowen for teaching me valuable courses. Their teaching has established the foundation of my research and provided me with several valuable insights. I have enjoyed many discussions with them from technical to non-technical topics.

My deepest love and gratitude dedicate to my parents and my wife, Tu Anh, for their support and devotion throughout my journey. Without their encouragement, this thesis would not have been finished.

Finally, I gratefully acknowledge the Natural Sciences and Engineering Research Council of Canada (NSERC), and the Department of Electrical and Computer Engineering at the University of Saskatchewan for their financial support of my studies.

Table of Contents

List of Tables

List of Figures

List of Abbreviations

5G	Fifth-Generation
ASK	Amplitude Shift Keying
AWGN	Additive White Gaussian Noise
BEP	Bit Error Probability
BER	Bit Error Rate
CIR	Channel Impulse Response
CP	Cyclic Prefix
CP-NFDM	Cyclic Prefix based Non-orthogonal Frequency Division Multiplexing
CP-OFDM	Cyclic Prefix based Orthogonal Frequency Division Multiplexing
DFT	Discrete Fourier Transform
FFT	Fast Fourier Transform
ICI	Inter-channel Interference
IDFT	Inverse Discrete Fourier Transform
IFFT	Inverse Fast Fourier Transform
IM	Index Modulation
IoT	Internet of Things
LTE	Long Term Evolution
ML	Maximum Likelihood
NB-IoT	Narrowband Internet of Things
NFDM	Non-orthogonal Frequency Division Multiplexing
NFDM-IM	Non-orthogonal Frequency Division Multiplexing with Index Modulation
OFDM	Orthogonal Frequency Division Multiplexing
OFDM-IM	Orthogonal Frequency Division Multiplexing with Index Modulation
OOB	Out-of-band
PAPR	Peak to Average Power Ratio
PSD	Power Spectrum Density
PSK	Phase Shift Keying
QAM	Quadrature Amplitude Modulation
RB	Resource Block

SEFDM	Spectrally Efficient Frequency Division Multiplexing
SNR	Signal to Noise Ratio
SVD	Singular Value Decomposition
TDL-D	Tapped Delay Line type D
WLAN	Wireless Local Area Network
ZP	Zero Padding
ZP-SEFDM	Zero Padding based Spectrally Efficient Frequency Division Multiplexing

1. Introduction

1.1 Introduction

Internet of Things (IoT) is a topic of great practical importance in the field of wireless communications [1–4]. As the name suggests, it refers to a massive communication network in which numerous devices are connected and exchange information. However, unlike high-rate applications such as video streaming over Wireless Local Area Networks (WLAN 802.11) or Long Term Evolution (LTE) mobile networks, many IoT systems are specifically designed for low-rate data transmission among terminals such as sensors and smart home devices [5]. These devices typically transmit or receive small packets of data sporadically, hence they are usually battery powered and last many years until the next refill or replacement. In other words, data rate is not a priority in most IoT systems.

Nevertheless, how to make the best use of bandwidth is always important when it comes to designing a real communication system. Indeed, with numerous devices operating in the same network, one must prepare for the scenario when all or many devices operate simultaneously. In such a situation, bandwidth allocation problem becomes challenging. For example, the Narrowband IoT (NB-IoT) standard provides a total amount of 180 kHz bandwidth and subcarrier spacing 3.75 or 15 kHz [5]. Using conventional techniques, the maximum number of simultaneously-operating devices is approximately equal to the number of subcarriers, which is up to 48 (180 kHz divided by 3.75 kHz). Obviously, the network has a good chance of experiencing data loss or outages when there are more devices than this maximum number attempting to transmit information at a given time. Therefore, it is desirable to increase the spectral efficiency of an IoT system in order to provide the ability to serve more devices within the fixed amount of bandwidth.

Orthogonal Frequency Division Multiplexing (OFDM) is a well-established technique in communications. Perhaps, its first widespread commercial use started in 1999 with the 802.11a standard for WLAN [6]. In 2008 it was adopted in the LTE standard for cellular telephone communications [7]. The advantage of this technique is hinted in its name: "orthogonal". In the time domain, an OFDM signal can be formed as a summation (superposition) of many orthogonal waveforms, namely harmonically-related sinusoidal carriers. The receiver can be designed to decode this composite signyc al and obtain data on every individual waveform without interference between carriers.

An OFDM signal in the frequency domain is illustrated in Fig. 1.1, which shows that the subcarriers can be packed in an overlapping manner with frequency separation (or subcarrier spacing) of $\Delta_f = \frac{1}{T_s}$, where T_s is the duration of an OFDM symbol. This value can be called the orthogonal limit since it is the smallest frequency separation for which orthogonality is achieved.

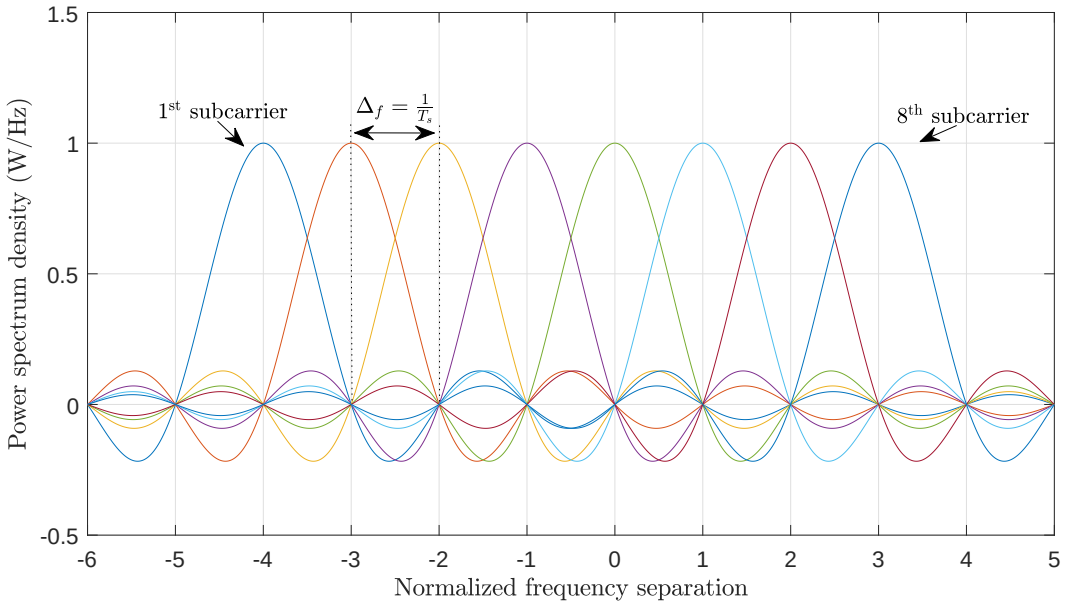

Figure 1.1: Overlapping subcarriers in OFDM.

Nevertheless, with the increasing demand for higher data rates under a fixed bandwidth, alternatives to OFDM are being considered. One interesting idea arises from a simple question: Can we make the subcarrier spacing even smaller than the orthogonal limit, hereby

reducing the bandwidth consumption?

Such a question leads to the topic of Non-orthogonal Frequency Division Multiplexing (NFDM) or Spectrally-Efficient Frequency Division Multiplexing (SEFDM) [8]. In the process of producing a transmit signal, one simply can reduce the frequency separation between the adjacent subcarriers and perform the remaining operations as in OFDM. However, in doing so, it is generally not possible to recover each waveform without suffering from interference among the subcarriers. As a matter of fact, the smaller the subcarrier spacing (beyond the orthogonal limit) is, the larger the interference is introduced [9]. A survey of research works done in this topic can be found in [8], which essentially suggests that NFDM is not ready to replace OFDM due mainly to its poor error performance resulting from the interference. However, recent efforts to re-design NFDM systems [10] have shown very promising results. Further integration of existing techniques designed for OFDM into NFDM scheme is also receiving a great attention from the research community [11–13].

On the other hand, by looking at Fig. 1.1 one can potentially exploit the spatial pattern of subcarriers. For example, by making one subcarrier inactivated, which is equivalent to carrying no data, the position of that carrier conveys meaningful information. Based on this observation, the concept of index modulation (IM) was introduced for OFDM [14,15]. In an OFDM-IM system, the information bits are divided into two streams, one for constellation mapping and one for determining active subcarriers. Generally, a reduced number of active channels means a less amount of data (namely constellation bits) being carried. However, this loss can be compensated by the data transmitted by means of subcarrier patterns (namely index bits). In some cases, a good compromise between constellation bits and index bits can be made to achieve an overall enhancement in the bit rate. In particular, this is possible for OFDM systems employing low modulation orders, which fit extremely well to the context of IoT. The principle of index modulation suggests that it should work with any multicarrier system, including NFDM, but the combination of index modulation and NFDM has not been studied in detail.

Motivated by the above discussion, the main objective of this thesis is to explore the combinations of index modulation and NFDM. Several important benchmarks to assess dif-

ferent communication systems such as bit error performance, spectral efficiency and power consumption are carefully taken into account. Overall, the results demonstrate the effectiveness of the investigated schemes. In particular, the proposed systems achieve better spectral efficiency than OFDM and OFDM-IM for low data rate and low power applications, such as IoT. The obtained results suggest better operating points by using the investigated/proposed systems than OFDM and OFDM-IM in the bandwidth-power plane.

1.2 Organization of the Thesis

This thesis is organized in a manuscript style. The first chapter provides the context of the thesis, which is the IoT applications. Communication techniques such as OFDM and index modulation are also discussed briefly to familiarize readers with the general topic of the thesis. Chapter 2 presents the fundamentals of OFDM and NFDM. The system model and detection strategies of index modulation are also included. Furthermore, power spectrum density (PSD) measurements of OFDM and NFDM are compared to highlight the potential advantage of NFDM.

Chapter 3 presents a novel combination of index modulation and fast OFDM, which is a variant of NFDM. This system is shown to outperform OFDM and OFDM-IM in terms of the bit rate. The detection error probability is derived and compared to that of OFDM. Based on the derived error probability, an optimized constellation is proposed, which improves the overall system error performance. Finally, at a fixed error rate, the proposed system is shown to achieve an equivalent spectral efficiency, but requiring less power as compared to OFDM.

The second manuscript presented in Chapter 4 introduces a novel design for NFDM systems. The main improvement in the proposed design is that interchannel interference, which is inevitable in the conventional NFDM design, is completely eliminated. It results in an NFDM system with the same bit error performance over an AWGN channel as an OFDM system, regardless of the subcarrier spacing compression factor. The power spectrum density of the new waveform is investigated, which leads to a new spectrum control method. Numerical results show that spectral efficiency enhancements can be achieved by using the proposed design over the conventional NFDM design.

Chapter 5 contains the final manuscript, which investigates a combination of the index modulation scheme in Chapter 3 and the proposed NFDM system in Chapter 4. The bit error probability of this system is derived, which suggests the use of an improved constellation to optimize the error performance. In terms of spectral efficiency performance, the proposed system can produce a 13% enhancement by using the optimized 8-QAM constellation. The results also show that index modulation for NFDM with high modulation orders does not yield any benefit in data rate.

Chapter 6 concludes the thesis by providing a brief summary of each chapter and discussing some potential future works in this area.

2. Background

This chapter describes the fundamental signal processing in OFDM systems, followed by a discussion on index modulation and its detection methods. The conventional implementation of NFDM in the literature is also included, where its spectrum is compared with that of an OFDM system. The purpose of this chapter is to provide readers with relevant background that serves as a foundation throughout the thesis.

2.1 Orthogonal Frequency Division Multiplexing

The block diagram of an OFDM system using Quadrature Amplitude Modulation (QAM) is presented in Fig. 2.1. First, the "S/P Converter" block arranges the incoming binary data (bits) into N parallel streams. The bits in each channel are modulated to symbols using QAM constellations. QAM constellations are most widely-used in OFDM thanks to their simple implementation and superior error performance over other constellations, especially with high modulation orders [16]. Each modulator implements mapping from bits to complex numbers (baseband symbols) in such a way that each possible set of bit values corresponds to a unique symbol. Denoting b as the number of bits in each group, then the total number of unique symbols is $M = 2^b$, which is often called the modulation order or modulation size. For a QAM constellation, all symbols can be represented on a two-dimension signal space (so-called constellation diagram). An example is given in Fig. 2.2 for $b = 4$ and $M = 16$. Each point or symbol in the constellation is formed by two components: In-phase (s_I) and Quadrature (s_Q) and can be represented in the form of a complex number $s_I + js_Q$. In Fig. 2.2, the real (in-phase) value is determined by the first 2 bits and the imaginary (quadrature) value is obtained from the last 2 bits. For instance, incoming bits of 0001 corresponding to

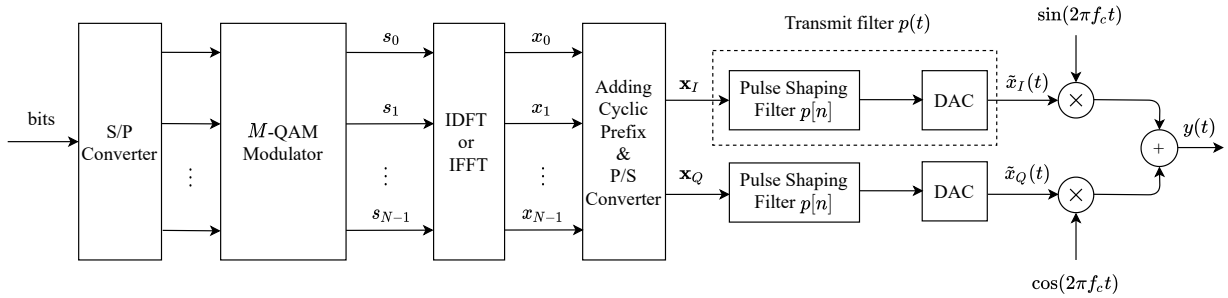

(a) Transmitter

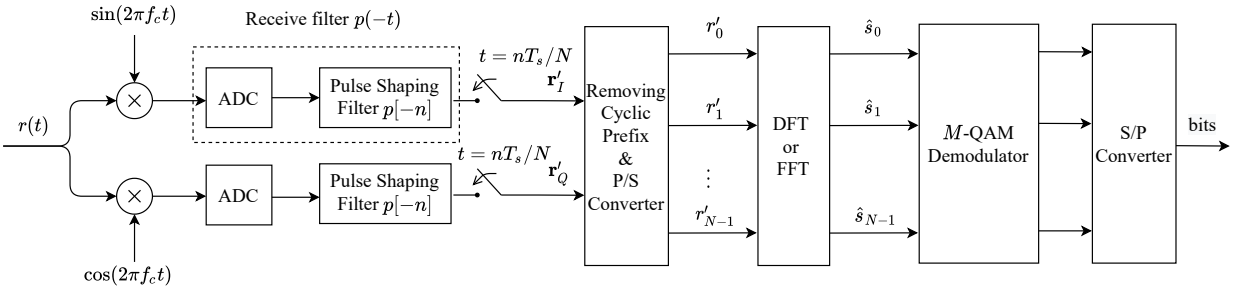

(b) Receiver

Figure 2.1: OFDM system block diagram.

the nth QAM symbol are mapped to a real value $s_{I,n} = -3$ and an imaginary value $s_{Q,n} = 1$, which produces a symbol $s_n = -3 + j$.

The N outputs of the N QAM modulators, denoted in the vector form as $\mathbf{s} = [s_0, \ldots, s_{N-1}]^T$, are connected to N inputs of an Inverse Discrete Fourier Transform (IDFT) block, yielding the output samples as

$$x_n = \frac{1}{\sqrt{N}} \sum_{k=0}^{N-1} s_k \exp\left(\frac{j2\pi nk}{N}\right), \quad 0 \le n \le N-1. \tag{2.1}$$

The resulting N complex time-domain samples can be collectively represented by a vector $\mathbf{x} = [x_n, \ldots, x_{N-1}]^{\mathrm{T}}$.

Then, an important procedure, namely cyclic prefix (CP) extension, is performed to ensure reliable transmission over a multipath channel. This operation creates a copy of the last N_{CP} samples and places them at the beginning of $\mathbf{x}$, producing vector $[x_{N-N_{\mathrm{CP}}}, \ldots, x_{N-1}, x_0, \ldots, x_{N-1}]$ of length $(N + N_{\mathrm{CP}})$. The real and imaginary parts of this signal are separated into two streams, denoted as $\mathbf{x}_I = \mathcal{R}\{\mathbf{x}\}$ and $\mathbf{x}_Q = \mathcal{I}\{\mathbf{x}\}$, respec-

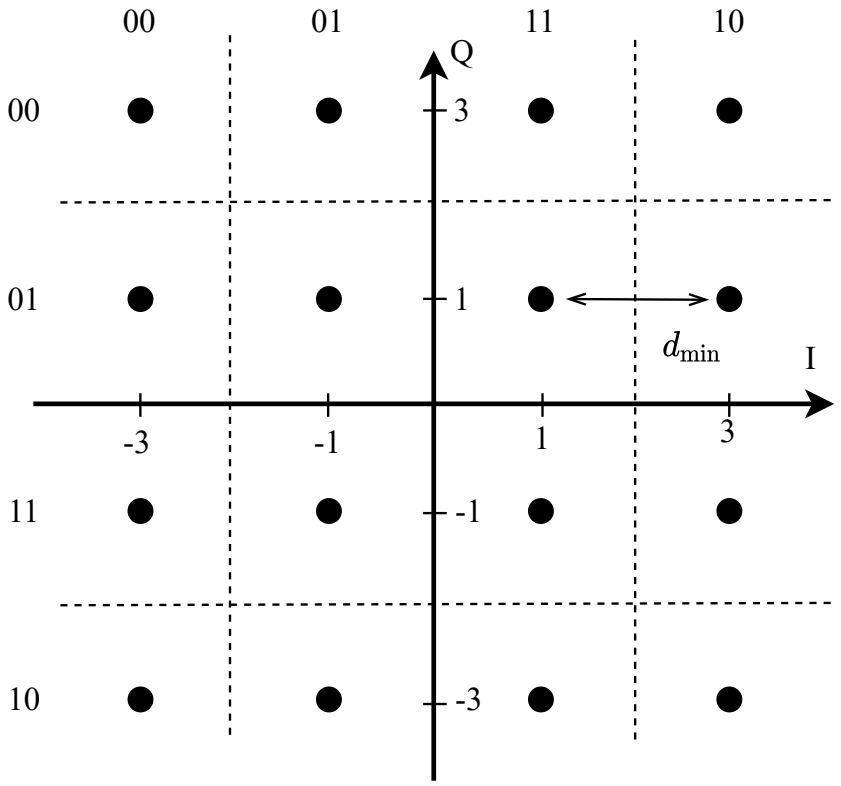

Figure 2.2: 16-QAM constellation.

tively. Then, a transmit filter $p(t)$ is applied on both parts, which essentially defines the spectrum shape of the transmit signal.

Let T_s be the duration of one OFDM symbol, not counting the CP length. Then, the time between two adjacent samples in $\mathbf{x}$ is $T_{\text{samp}} = \frac{T_s}{N}$, which is also known as the sampling period. Then, the transmitted signal in one symbol duration is given as

$$y(t) = \underbrace{\sum_{n=0}^{\hat{N}-1} x_{I,n} p(t - nT_{\text{samp}})}_{\tilde{x}_I(t)} \sin(2\pi f_c t) + \underbrace{\sum_{n=0}^{\hat{N}-1} x_{Q,n} p(t - nT_{\text{samp}})}_{\tilde{x}_Q(t)} \cos(2\pi f_c t) \tag{2.2}$$

where $\hat{N} = N + N_{\text{CP}}$ and f_c is the desired center frequency on which the signal is transmitted.

This signal is propagated through a multipath fading channel and arrives at the receiver, where the corrupted signal is expressed as

$$r(t) = \sum_{l=0}^{L-1} a_l(t) y(t - \tau_l) + w(t). \tag{2.3}$$

where $w(t)$ is additive white Gaussian noise (AWGN), $a_l(t)$ is the channel gain of the lth path ($0 \leq l \leq L-1$) and τ_l is the time delay associated to that path. Then, $r(t)$ is down-converted to baseband and filtered to remove high frequency components. Next, a matched filter $p(-t)$ is applied, whose output is sampled every $nT_{\text{samp}} = nT_s/N$ ($0 \leq n \leq \hat{N}-1$) second to produce a discrete-time sequence $\mathbf{r'} = [r'_0, \ldots, r'_{N+N_{\text{CP}}+L-2}]$, where [17]

$$r'_n = \sum_{l=0}^{L-1} a_{l,n} x_{n-l} + w_n, \tag{2.4}$$

with $a_{l,n}$ being the discrete-time channel gain corresponding to the lth tap and nth sample and w_n is the n sample of the filtered noise.

In the context of IoT applications where the devices are relatively static, the channel is considered constant over a long period of time $T_c \gg T_s$ (i.e., the coherence time T_c is much longer than the symbol duration). Then $a_{l,n}$ stays the same for many samples and (2.4) simplifies to

$$r'_n = \sum_{l=0}^{L-1} a_l x_{n-l} + w_n. \tag{2.5}$$

The above equation shows that each sample of the received signal depends on L samples of the transmitted signal. The length of received sequence $\mathbf{r'}$ is $N + N_{\text{CP}} + L - 1$, in which the first $N + N_{\text{CP}}$ are obtained from the $N + N_{\text{CP}}$ transmitted samples, while the last $L-1$ samples are generated by the effect of the multipath channel. As a result, this extra portion falls into the frame of the next OFDM symbol and introduces interference. However, it can be shown that if the CP length is chosen such that $L \leq N_{\text{CP}}$, one can simply remove the prefix of the received sequence to eliminate undesirable interference from the previous symbol [18].

Then, a N-point DFT is applied to the CP-removed vector to regenerate the frequency domain symbols $\hat{\mathbf{s}} = [\hat{s}_0, \ldots, \hat{s}_{N-1}]$, which are related to the transmit QAM symbols as [17]

$$\hat{s}_n = h_n s_n + \tilde{w}_n \tag{2.6}$$

where $h_n = \sum_{m=0}^{N-1} a_m \exp(-j2\pi mn/N)$ is the frequency response of the channel and $a_m = 0$ with $m \geq L$. Furthermore, it can be shown that the noise samples $\tilde{w}_n$ are independent and

identically-distributed zero-mean complex Gaussian variables with variance N_0, denoted as $\tilde{w}_n \sim \mathcal{CN}(0, N_0)$. Equation (2.6) shows that an OFDM signal can be decomposed into N parallel independent subchannels without inter-carrier interference (ICI). Before symbols are decoded, they need to be scaled as (i.e., by using a single-tap channel equalizer)

$$\frac{\hat{s}_n}{h_n} = s_n + \frac{\tilde{w}_n}{h_n}. \tag{2.7}$$

Finally, a QAM demodulator decodes $\frac{\hat{s}_n}{h_n}$ into bits by projecting it on the signal space and looking for the closest signal point in terms of the Euclidean distance. If the constellation is rectangular QAM such as the one in Fig. 2.2, the demodulator can alternatively implement the decision boundaries, shown as dashed-lines in the diagram, to decide which symbol is transmitted given a received signal point.

Matrix Representation of OFDM

An OFDM transceiver can be conveniently modelled as a linear system when only discrete-time baseband operations are considered. The post IDFT signal sequence is expressed in vector form as

$$\mathbf{x} = \mathbf{F}\mathbf{s}, \tag{2.8}$$

where $\mathbf{F}$ is the size-N IDFT matrix, whose element at the nth row and kth column is $f_{n,k} = \frac{1}{\sqrt{N}} \exp(j2\pi(n-1)(k-1)/N)$. Then the transmit OFDM symbol after CP insertion is given as

$$\mathbf{y} = [x_{N-N_{\mathrm{CP}}}, \ldots, x_{N-1}, x_0, \ldots, x_{N-1}]. \tag{2.9}$$

The received signal is then shown as

$$\mathbf{r}' = \mathbf{h} * \mathbf{y} + \mathbf{w}, \tag{2.10}$$

where $\mathbf{w} \sim \mathcal{CN}(0, N_0\mathbf{I})$, $\mathbf{I}$ is the identity matrix, $\mathbf{h} = [a_0, \ldots, a_{L-1}]$ is the channel gain vector and $*$ denotes convolution. Note that the length of $\mathbf{r}'$ is $N + N_{\mathrm{CP}} + L - 1$. Since the first N_{CP} and last $L-1$ samples are not used for detection, $\mathbf{r}'$ is truncated to length N, which is

$$\mathbf{r} = \mathbf{H}\mathbf{x} + \mathbf{w}, \tag{2.11}$$

where

$$\mathbf{H} = \begin{bmatrix} a_0 & \dots & \dots & 0 & a_{L-1} & \dots & a_1 \\ \vdots & \ddots & & & \ddots & \ddots & \vdots \\ \vdots & & \ddots & & & \ddots & a_{L-1} \\ a_{L-1} & \ddots & & & & & 0 \\ 0 & \ddots & \ddots & & \ddots & & \vdots \\ \vdots & & \ddots & \ddots & & \ddots & 0 \\ 0 & \dots & 0 & a_{L-1} & \dots & \dots & a_0 \end{bmatrix}_{N \times N} \tag{2.12}$$

is a circulant channel matrix. Such a matrix can be decomposed using the IDFT matrix as $\mathbf{H} = \mathbf{F}\mathbf{\Lambda}\mathbf{F}^{\mathrm{H}}$ where $(\cdot)^{\mathrm{H}}$ denotes the Hermitian operation, $\mathbf{\Lambda}$ is a diagonal matrix with diagonal elements $\mathbf{F}^{\mathrm{H}}\mathbf{h}'$, $\mathbf{h}' = [a_0, \dots, a_{L-1}, 0, \dots, 0]_{N \times 1}$. It follows that received signal $\mathbf{r}$ can be rewritten as

$$\mathbf{r} = \mathbf{F}\mathbf{\Lambda}\mathbf{F}^{\mathrm{H}}\mathbf{x} + \mathbf{w} = \mathbf{F}\mathbf{\Lambda}\mathbf{F}^{\mathrm{H}}\mathbf{F}\mathbf{s} + \mathbf{w} = \mathbf{F}\mathbf{\Lambda}\mathbf{s} + \mathbf{w} \tag{2.13}$$

At the receiver, the corresponding DFT matrix $\mathbf{F}^{\mathrm{H}}$ is performed on $\mathbf{r}$, yielding

$$\hat{\mathbf{s}} = \mathbf{F}^{\mathrm{H}}\mathbf{r} = \mathbf{F}^{\mathrm{H}}\mathbf{F}\mathbf{\Lambda}\mathbf{s} + \mathbf{F}^{\mathrm{H}}\mathbf{w} = \mathbf{\Lambda}\mathbf{s} + \tilde{\mathbf{w}}, \tag{2.14}$$

where $\mathbf{F}^{\mathrm{H}}\mathbf{F} = \mathbf{F}^{-1}\mathbf{F} = \mathbf{I}$ and $\tilde{\mathbf{w}}$ has the same statistics as $\mathbf{w}$. Finally, the single-tap equalization can be done on the nth subchannel as

$$\frac{\hat{s}_n}{\Lambda_{n,n}} = s_n + \frac{\tilde{w}_n}{\Lambda_{n,n}}. \tag{2.15}$$

In this representation, it can also be observed that there is no ICI affecting the demodulation process, as QAM demodulation can be performed independently on each equalized symbol.

Performance of OFDM over AWGN Channels

The overall error performance of an OFDM system is determined by average the average error over all N subchannels. As presented earlier in this section, an OFDM system can be treated as a set of independent parallel subchannels over AWGN channels without ICI.

Table 2.1: BEP expressions for different constellations.

Constellation	BEP
BPSK	$Q(\sqrt{2\gamma_b})$
QPSK (4-QAM)	$\approx Q(\sqrt{2\gamma_b})$
Hexagonal 8-QAM	$\approx \frac{1}{3}\left(\frac{13}{4}Q\left(\sqrt{\frac{4}{3}\gamma_b}\right) + 1.5Q^2\left(\sqrt{\frac{8}{9}\gamma_b}\right) - \frac{9}{2}Q\left(\sqrt{\frac{4}{3}\gamma_b}\right)Q\left(\sqrt{\frac{4}{9}\gamma_b}\right)\right)$
16-QAM	$1-\left(1-1.5Q(\sqrt{0.8\gamma_b})\right)^2$

Therefore, the bit error probability (BEP) of an OFDM system is the same as the BEP of the employed constellation [1].

The BEP expressions of various constellations are given in Table 2.1 [18, 19]. In these expressions, γ_b is the signal-to-noise ratio (SNR) per bit and $Q(x) = \frac{1}{2\pi}\int_x^\infty \exp(-u^2/2)du$ is the Q-function. The BEP curves of the investigated constellations are compared in Fig. 2.3. It can be seen that when the modulation order increases, the system error performance becomes worse if γ_b is held fixed. The exception is going from BPSK ($M = 2$) and QPSK ($M = 4$) when both constellations yield exactly the same BEP. This is because a QPSK signal is essentially the sum of two orthogonal (in-phase and quadrature) BPSK signals. For instance, at $\gamma_b = 10$ dB, BPSK and QPSK obtain the BEP of 4×10^{-6} while these numbers are 10^{-4} for Hex 8-QAM and 7×10^{-3} for 16-QAM. In general, performance degradation in using a larger QAM constellation is because of the simple fact that, for the same signal power (per bit) a larger constellation is a more crowded constellation, making the minimum distance among constellation points smaller, which likely results in more erroneous detection decisions under the same noise condition.

Nevertheless, by sacrificing error performance or affording higher transmit power, higher spectral efficiency can be achieved when increasing the modulation order. First, define the

[1] In general, this statement is only true in the case of AWGN channels.

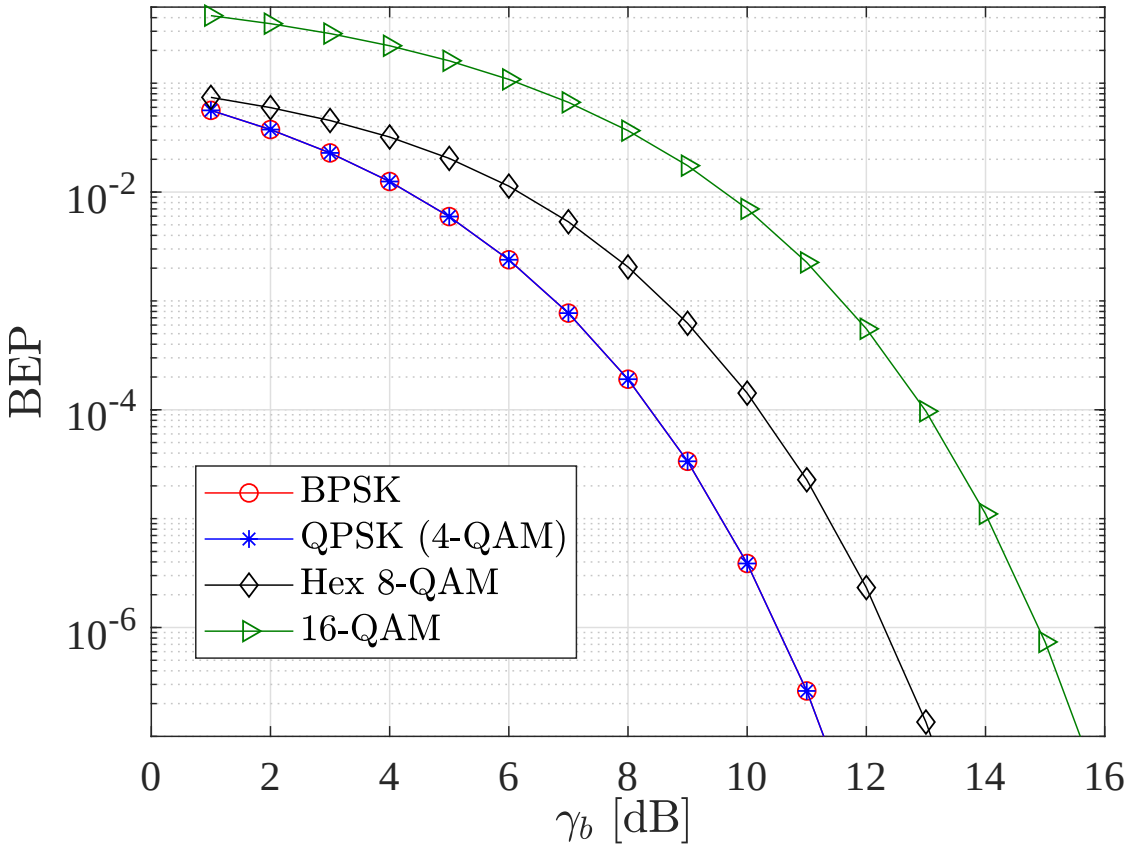

Figure 2.3: BEP of constellations

spectral efficiency of an OFDM system as [2]

$$\eta = \frac{r_b}{T_s B} \quad \text{[bits/s/Hz]}, \tag{2.16}$$

where $r_b = N \log_2 M$ is the number of bits transmitted in one OFDM symbol, $B = \frac{N}{T_s}$ is the (approximate) occupied bandwidth, T_s is the symbol duration and N is the number of subcarriers. It can be seen that $\eta = \log_2 M$, confirming that the spectral efficiency of an OFDM system is equal to that of a single-carrier transmission system using a constellation of size M. For instance, an OFDM system using 16-QAM constellation has the spectral efficiency of 4 bits/s/Hz.

Before presenting spectral efficiency comparison among different systems/constellations, we review below an important benchmark, namely the Shannon's normalized channel capacity, which is given as [16]

$$\eta_{\text{lim}} = \log_2 (1 + \eta_{\text{lim}} \gamma_b) \quad \text{[bits/s/Hz]}. \tag{2.17}$$

In essence, η_{lim} gives the maximum spectral efficiency of a communication system operating at an SNR per bit of γ_b and with an arbitrarily small error probability. Such a system, however, requires the use of very complicated/advanced modulation schemes. In other words, for a system with spectral efficiency $\eta > \eta_{\text{lim}}$, it is not possible to achieve an arbitrarily small error probability regardless of the modulation scheme used. Therefore, η_{lim} can serve as a reference when assessing the spectral efficiency of different communication systems and modulation schemes.

Comparison of the spectral efficiency versus the required SNR per bit is presented in Fig. 2.4 for four constellations: BPSK, QPSK, Hex 8-QAM and 16-QAM. In this comparison, the target BEP is taken at 10^{-6}, i.e., all four constellations are assessed at the target BEP of 10^{-6}. Given the four operating points in the figure, it is clear that 16-QAM constellation obtains the highest spectral efficiency (4 bits/s/Hz at $\gamma_b = 14.9$ dB) where BPSK is the most spectrally-inefficient modulation scheme (1 bit/s/Hz at $\gamma_b = 10.5$ dB). In particular, using QPSK

[2]Since AWGN channels are the focus of this discussion, techniques such as coding and cyclic prefix extension are not taken into account in quantifying this term.

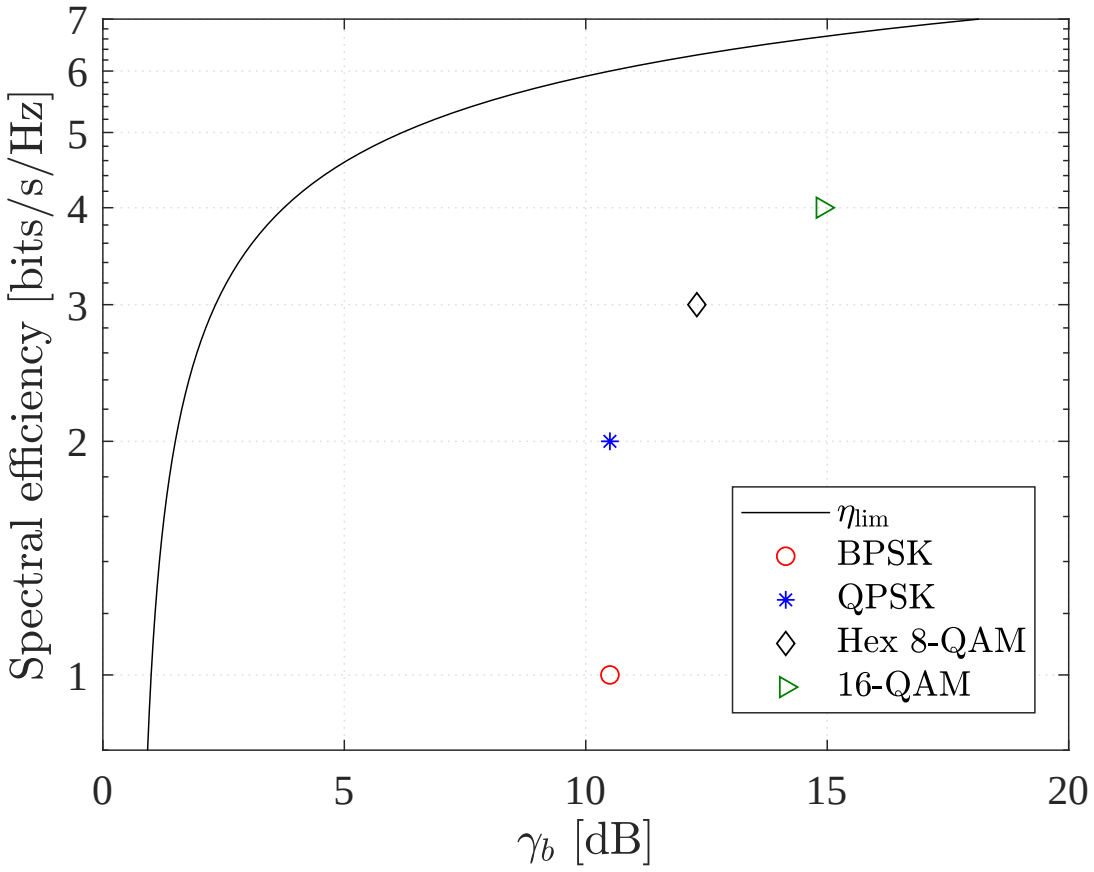

Figure 2.4: Spectral efficiency comparison of different modulation schemes.

can achieve twice as much efficiency as BPSK but requiring the same power (2 bits/s/Hz also at $\gamma_b = 10.5$ dB). It is pointed out, however, that the comparison does not obviously suggest using any modulation scheme over the remaining schemes, but provides a guideline for designing certain communication systems. For example, high data rate applications such as video streaming usually need moderate to high spectral efficiency, hence requiring large modulation orders and more transmit power than low rate applications such as IoT, where smaller modulation orders are sufficient.

2.2 Non-orthogonal Frequency Division Multiplexing

NFDM is expected to offer a significant improvement compared to OFDM in terms of spectral efficiency. In order to achieve such enhancement, the occupied bandwidth in NFDM is packed more compactly than OFDM by reducing the subcarrier spacing. This is illustrated in Fig. 2.5, where subcarrier arrangements of OFDM and NFDM in the frequency domain are compared when the same number of subcarriers, N, is used in both systems. First, let $\alpha < 1$ be a compression factor, which defines the ratio of subcarrier spacing in NFDM to that in OFDM. In OFDM, the relationship between subcarrier spacing Δ_f and bandwidth B is

$$B = N\Delta_f = \frac{N}{T_s}. \tag{2.18}$$

As mentioned, the subcarrier spacing in NFDM is intentionally reduced by a factor of α, making the occupied bandwidth in this system as

$$B = \Delta_f + \alpha\Delta_f(N-1). \tag{2.19}$$

It can be seen that, when comparing NFDM and OFDM with the same number of subcarriers N, NFDM signal occupies a smaller bandwidth than OFDM whenever $\alpha < 1$. Alternatively, the same amount of bandwidth allows more subcarriers in NFDM than in OFDM. This potentially results in a higher bit rate, hence improves the spectral use (or spectral efficiency, measured in bits/s/Hz).

Although Eq. (2.19) indicates that one can reduce the occupied bandwidth by adjusting the compression factor α, the error performance of NFDM might not be the same as in

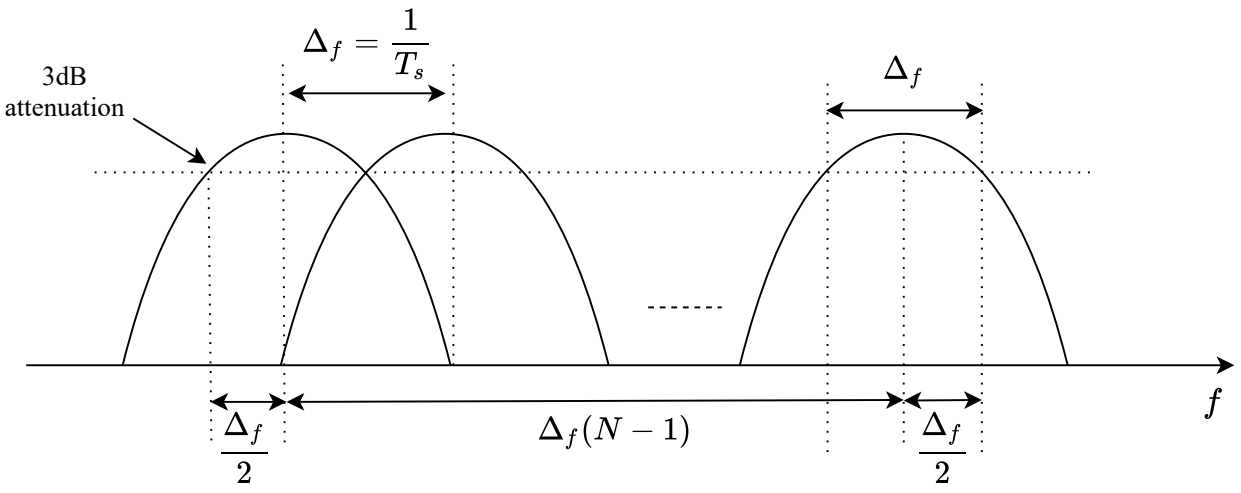

(a) OFDM

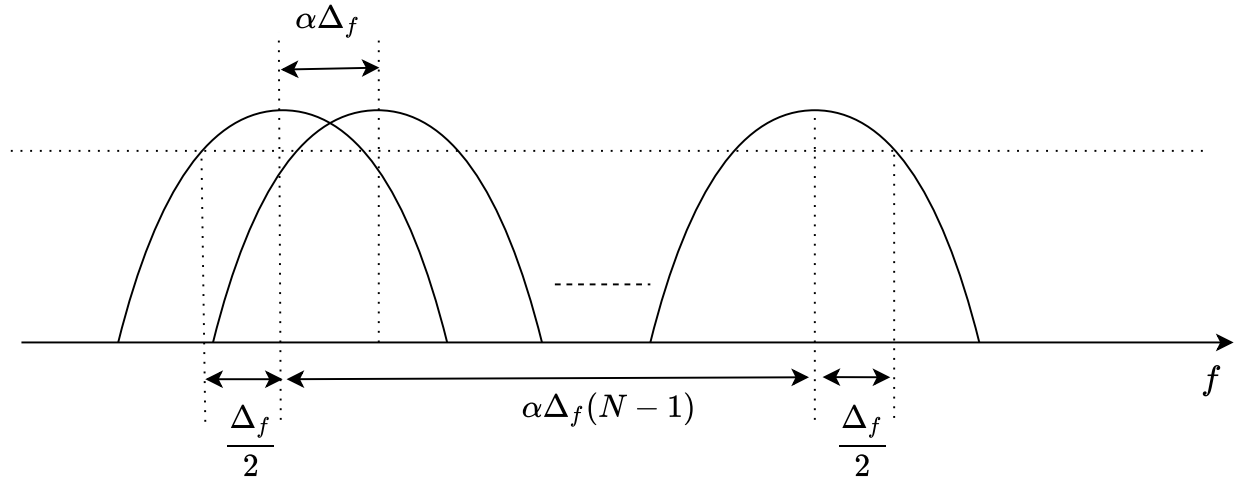

(b) NFDM

Figure 2.5: Bandwidth compression in NFDM

OFDM. In fact, lowering α introduces cross channel interference and severely contaminates the signal at the receiver.

The most straightforward way to realize an NFDM system is to modify the conventional OFDM transceiver. Fig. 2.6 presents a conventional NFDM system block diagram, where cyclic prefix is omitted and the simple AWGN channel is considered.

As highlighted in the figure, the only change needed to reflect compression factor α is to

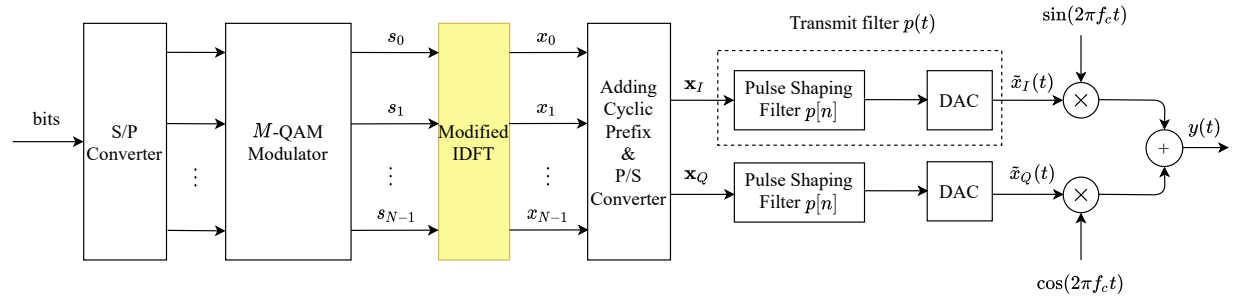

(a) Transmitter

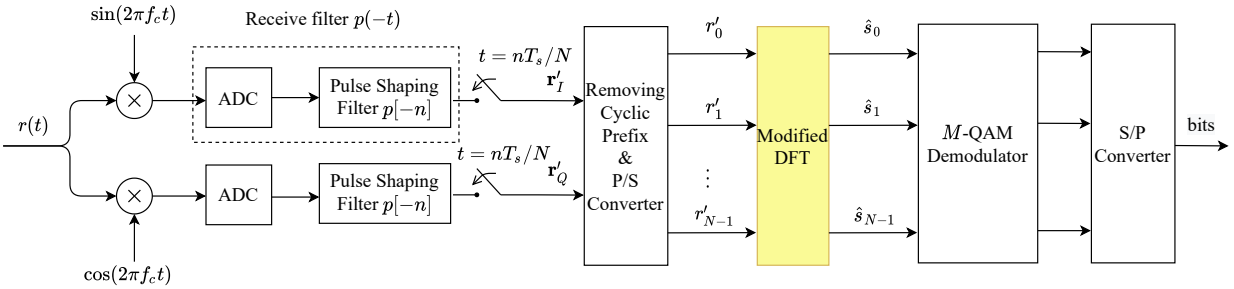

(b) Receiver

Figure 2.6: NFDM system block diagram.

modify the IDFT/DFT pair. Specifically, the post-IDFT signal is expressed as

$$x[n] = \frac{1}{\sqrt{N}} \sum_{k=0}^{N-1} s[k] \exp\left(\frac{j2\pi nk}{N}\alpha\right), \quad 0 \le n \le N-1 \tag{2.20}$$

or in matrix form

$$\mathbf{x} = \mathbf{F}\mathbf{s}, \tag{2.21}$$

where the so-called modified IDFT matrix $\mathbf{F}$ is now defined by its element in the nth row and kth column as $f_{n,k} = \frac{1}{\sqrt{N}} \exp(j2\pi nk\alpha/N)$. At the receiver, the input-output model is similar to OFDM, which is

$$\mathbf{r} = \mathbf{F}\mathbf{s} + \mathbf{w}, \tag{2.22}$$

where $\mathbf{w} \sim \mathcal{CN}(0, N_0\mathbf{I})$. Next, the corresponding modified DFT $\mathbf{F}^{\mathrm{H}}$ is applied in an attempt to recover $\mathbf{s}$, resulting in

$$\hat{\mathbf{s}} = \mathbf{F}^{\mathrm{H}}(\mathbf{F}\mathbf{s} + \mathbf{w}). \tag{2.23}$$

Unfortunately, $\mathbf{F}^{\mathrm{H}} \neq \mathbf{F}^{-1}$ in the case of NFDM, which leads to

$$\hat{\mathbf{s}} = \mathbf{C}\mathbf{s} + \tilde{\mathbf{w}}, \tag{2.24}$$

where $\tilde{\mathbf{w}} = \mathbf{F}^{\mathrm{H}}\mathbf{w}$ follows the same distribution as $\mathbf{w}$ and $\mathbf{C} = \mathbf{F}^{\mathrm{H}}\mathbf{F}$ is the correlation matrix whose form is a Toeplitz matrix. Specifically, this correlation matrix can be represented as

$$\mathbf{C} = \begin{bmatrix} 1 & c_1^* & \dots & c_{N-1}^* \\ c_1 & 1 & \ddots & \vdots \\ \vdots & \ddots & \ddots & c_1^* \\ c_{N-1} & \dots & c_1 & 1 \end{bmatrix}, \tag{2.25}$$

where $()^*$ denotes complex conjugate operation and c_k is given as [9]

$$c_k = \frac{1}{N}\frac{1-\exp(j2\pi k\alpha)}{1-\exp(j2\pi k\alpha/N)}, \quad 0 \le k \le N-1. \tag{2.26}$$

Since the values of $\{c_1, \dots, c_{N-1}\}$ are not zeros when $\alpha < 1$, ICI presents in the system and destroys the subcarrier orthogonality. This issue becomes more severe when further decreasing compression factor which results in poor signal recovery performance, hence limits the use of NFDM in practice.

As expected, the best error performance of NFDM is obtained when the maximum likelihood (ML) receiver is employed. Given the contaminated signal in Eq. (2.24), the ML solution is found as

$$\hat{\mathbf{s}}_{\mathrm{ML}} = \arg\min_{\mathbf{s}\in\mathcal{S}} ||\hat{\mathbf{s}} - \mathbf{C}\mathbf{s}||^2, \tag{2.27}$$

where $\mathcal{S}$ is the set (codebook) containing all possible values of the QAM symbol vector $\mathbf{s}$ (codewords). This detector searches for a codeword that is "nearest" to the received vector $\hat{\mathbf{s}}$ by minimizing the Euclidean distance between $\hat{\mathbf{s}}$ and $\mathbf{C}\mathbf{s}$. Although such a detector yields the optimal performance, examining the entire codebook is neither hardware nor time efficient, especially when the codebook size is large. Therefore, this approach is clearly not feasible in practice. This motivates us to come up with a different design to reduce the complexity and/or improve error performance of NFDM. Our contribution along this line is presented in Chapter 4.

2.3 Index Modulation

2.3.1 System Model

As mentioned briefly in Chapter 1, index modulation was proposed to be used with OFDM to improve the spectral efficiency and/or error performance. The principle of this technique is to exploit another dimension (pattern of active subcarriers) to carry a portion of data. However, a good trade-off must be investigated to obtain the best data rate, as "extra" bits obtained by means of active subcarrier patterns generally comes with a reduction in the number of constellation bits.

Consider an OFDM system with index modulation (OFDM-IM), with N total subcarriers and K out of them are activated. The indexing procedure can be described as in Fig. 2.7. First, incoming bits are divided into two groups containing λ_1 and λ_2 bits, respectively. Here λ_2 bits are called index bits, which determine the set of K active subchannels (denoted as $\mathcal{K}$) to carry QAM symbols. When $\mathcal{K}$ is decided, the switches corresponding to active channels are closed, which allow input bits to be fed in QAM modulators, producing K complex symbols. As a result of being disconnected, the remaining $N-K$ subchannels are left unused, or equivalently carry symbol zeros. The input of the IDFT block thus can be expressed as

$$\mathbf{s} = [s_0, \ldots, s_{N-1}]^{\mathrm{T}}, \tag{2.28}$$

where $()^{\mathrm{T}}$ denotes the transpose operation and s_n either belongs to a QAM constellation or is zero, depending on whether the nth channel is activated or not. It is clear that the total number of bits conveyed in $\mathbf{s}$ is

$$\lambda = \lambda_1 + \lambda_2 = \sum_{k=0}^{K-1} \log_2(M_k) + \left\lfloor \log_2 \begin{pmatrix} N \\ K \end{pmatrix} \right\rfloor, \tag{2.29}$$

where M_k is the size of the QAM constellation used in the kth active subcarrier, $\lfloor \cdot \rfloor$ denotes the floor function and $\begin{pmatrix} N \\ K \end{pmatrix} = \frac{N!}{K!(N-K)!}$ is the "N choose K" combination (or binomial coefficient). Usually, the total number of subcarriers N is fixed, so the value of K must be carefully chosen (see Chapter 3) to obtain the maximum overall bit rate.

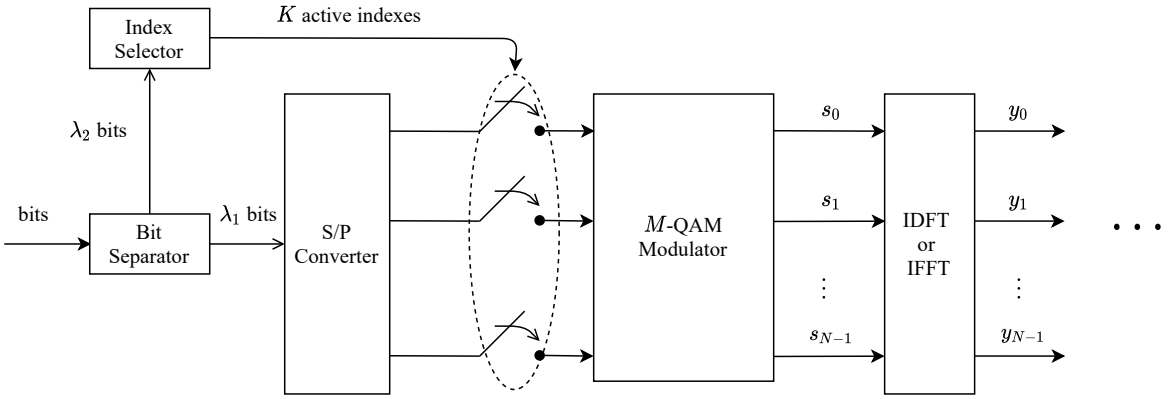

(a) Transmitter

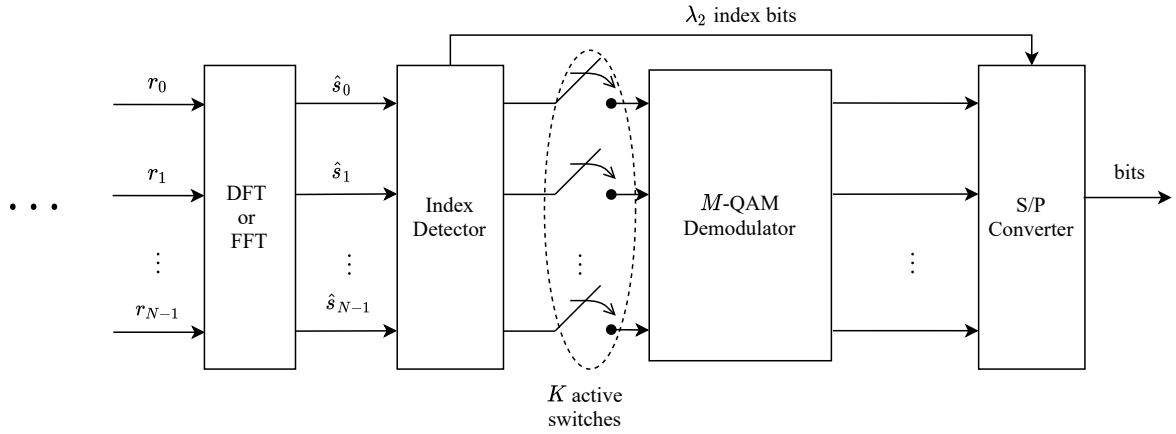

(b) Receiver

Figure 2.7: OFDM-IM block diagram.

2.3.2 Detection Methods

There are two detection strategies which have been widely considered for OFDM-IM. The first one uses the maximum likelihood receiver, which delivers the best possible error performance. The ML receiver searches over all possible realizations of the transmit signal $\mathbf{s}$ (codewords) in a pre-defined set $\mathcal{S}$ (codebook) to find the one that is closest to $\hat{\mathbf{s}}$ [20]:

$$\mathbf{s}' = \underset{\mathbf{s}\in\mathcal{S}}{\operatorname{argmin}} ||\hat{\mathbf{s}} - \mathbf{s}||^2 = \underset{\mathbf{s}\in\mathcal{S}}{\operatorname{argmin}} \sum_{n=0}^{N-1} |\hat{s}_n - s_n|^2. \tag{2.30}$$

As the ML receiver runs though all possible codewords, its computational complexity is determined by the size of codebook, which is $\binom{N}{K} M^K$. For example, with $M = 2$, $N = 12$

and $K = 11$, the codebook has $24,576$ codewords. However, if constellation size is $M = 4$, then the size is $50,331,648$. This means that even a small increase in the constellation size can lead to a huge expansion of $\mathcal{S}$ and rule out the use of the ML receiver in practice.

Therefore, one is interested in a more efficient method such as a two-stage detector in [14, 20]. To avoid the high complexity of jointly deciding which subcarriers are active and decoding the constellation points on the those subcarriers as in the ML receiver, this detector splits the detection process as follows: the active subchannels are found in the first stage, followed by parallel symbol demodulation in the second stage. The first stage occurs after the execution of DFT, i.e., applies to signal $\hat{\mathbf{s}}$. The criterion to find active subcarriers relies on the fact that there are only K non-zero symbols being carried in $\mathbf{s}$ and $\hat{\mathbf{s}}$ is simply the AWGN-corrupted version of $\mathbf{s}$. Therefore, by examining all N magnitude values in $\hat{\mathbf{s}}$, the $N - K$ smallest values can be found and identified as inactive subchannels. Then, one can independently demodulate the QAM symbols on the K active subcarriers.

Obviously, this two-stage detection method implements signal detection on each subchannel, rather than an exhaustive search over the entire set of channels, hence reducing the complexity significantly compared to the ML receiver. However, the problem with this method is error propagation across two stages. In particular, if the active subcarriers pattern is incorrectly recognized, the next detection stage likely experiences more errors. For example, in an OFDM-IM with $N = 12$ and $K = 4$, the set of active subcarriers could be $\mathcal{K} = \{1, 2, 3, 4\}$. Suppose that due to the noisy channel, the detected pattern at the receiver using the two-step procedure is $\hat{\mathcal{K}} = \{1, 2, 3, 5\}$. In this case, QAM symbols from the first three channels will be correctly demodulated, however the information in the 5th channel is not an actual transmitted symbol, hence the bits recovered from the 5th channel with have an error probability of $\frac{1}{2}$. This is the major drawback of two-stage detection compared to the ML detection.

Ideally, if there is no erroneous decision at the first stage, the probability of making an error in the next stage will be merely the error probability of the QAM constellation, which makes the overall error performance of OFDM-IM equal to that in OFDM. However, such idealistic scenario is unrealistic because the index detection performance relies on the

minimum distance d_0 from all constellation points to the origin, which could be smaller than minimum distance $d_{\min}$ of the constellation. Therefore, it is reasonable to investigate the best trade-off between d_0 and $d_{\min}$ for index modulation to work efficiently. Our contribution on this matter is presented in Chapter 3 for a special variant of OFDM, and further expanded in Chapter 5 for NFDM.

2.4 Power Spectrum Density

In this subsection, the advantage of NFDM compared to OFDM in terms of occupied bandwidth is further demonstrated by comparing their transmitted power spectrum densities (PSD). Loosely speaking, PSD is a power response of a signal in the frequency domain, which shows how the average power is distributed as a function of frequency. Generally, the PSD of a signal $x(t)$ can be obtained by averaging the magnitude squareds of its Fourier transform observed over a very long time, which is expressed as

$$P_x(f) = \lim_{T\to\infty} \frac{1}{T} E\{|\mathcal{F}\{x(t)\}|^2\}, \tag{2.31}$$

where E and $\mathcal{F}$ denote expectation and Fourier transform functions, respectively.

To compare the PSDs of OFDM and NFDM, some parameters need to be set, including the total number of symbols N, symbol duration T_s and the type of transmit filter $p(t)$. In this demonstration, these parameters are adopted from WLAN 802.11a [6], which specifies $N = 64$, $T_s = \frac{1}{312.5\text{kHz}} = 3.2\mu s$, and a rectangular transmit filter $p(t)$, defined as

$$p(t) = \begin{cases} 1, & -T_s/2 \le t < T_s/2 \\ 0, & \text{otherwise} \end{cases}. \tag{2.32}$$

According to the standard, the subcarrier spacing is $\Delta_f = 312.5$ kHz, resulting in an occupied bandwidth according to Eqs. (2.18) and (2.19) as $B = 64 \times 312.5$ kHz $= 20$ MHz for OFDM and $B' = 312.5 \times 10^3(1 + 0.5 \times 63) \approx 10$ MHz for NFDM with compression factor $\alpha = 0.5$.

The PSDs of OFDM and NFDM are compared in Fig. 2.8 using computer simulations. The first observation is that the occupied bandwidths observed in the figure agree with the above calculated values. Having the same number of subcarriers, hence same bit rate, NFDM

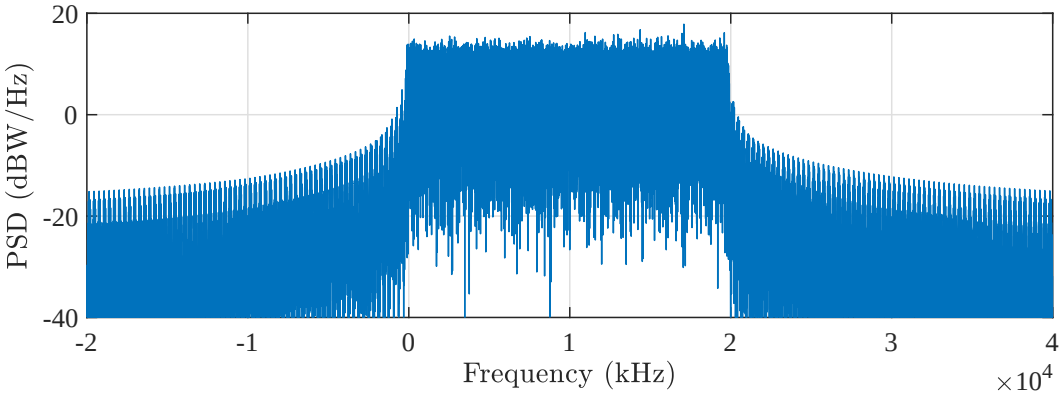

(a) OFDM

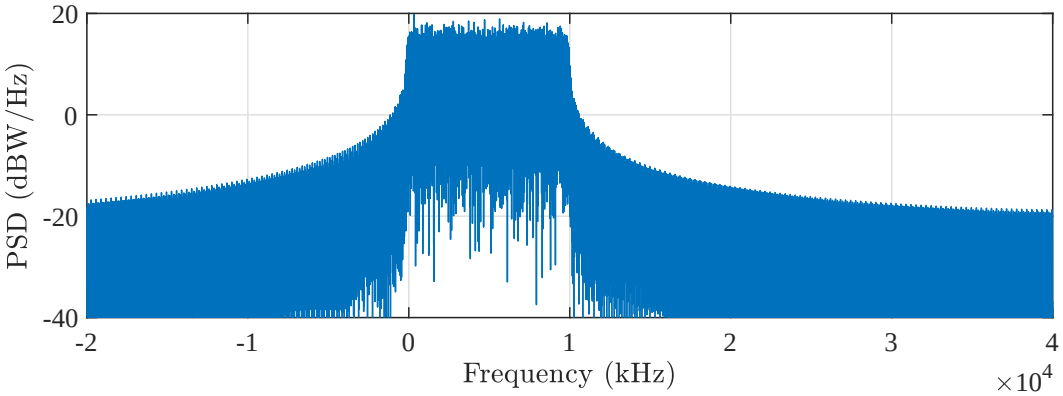

(b) NFDM $\alpha = 0.5$

Figure 2.8: PSD comparison between OFDM and NFDM

with $\alpha = 0.5$ only takes up approximately half of the bandwidth required in OFDM, which is 10 MHz and 20 MHz, respectively. To compare the spectral efficiency, first recall that

$$\eta = \frac{\text{Bit rate}}{\text{Symbol duration} \times \text{Bandwidth}} \quad [\text{bits/s/Hz}]. \tag{2.33}$$

It is obvious that the bit rate and symbol duration of two systems are identical in this comparison, so bandwidth becomes as the deciding factor. Given the clear advantage in saving bandwidth, NFDM appears to be the winner against OFDM in terms of spectral efficiency. However, to obtain a meaningful comparison, both systems must deliver the quality of service, i.e., requiring the same transmit power to achieve the same bit error rate (BER). In the OFDM system, orthogonality among subchannels is preserved, therefore the BER of the system is the average BER over all subchannels. In a special case when all subchannels use the same constellation, then the BER of an OFDM system is the BER of the constellation. Meanwhile, due to ICI, each subchannel in the NFDM system is contaminated by other subchannels and hence more prone to errors than in the OFDM system. The result is that NFDM generally suffers from worse error performance compared to OFDM. Therefore, despite occupying a smaller bandwidth, the true spectral efficiency of an NFDM system might not be better that of an OFDM system when the error performance is taken into account.

The second observation is that the two PSDs have similar shapes despite different occupied bandwidths. Let's classify two areas in the spectra: the portion where the majority of the transmit signal power lies on (in-band region) and the rest where the signal power is spread out (out-of-band region). In both systems, the average signal power is 0 dBW in the in-band region and gradually reduces to -30 dBW in the out-of-band region. This is to say, NFDM can meet spectrum requirements that are imposed on OFDM. In Chapter 4, a new spectrum control technique is introduced for NFDM that can further reduce the signal power in the out-of-band region, increasing its suitability for practical applications.

2.5 Narrowband Internet of Things

This thesis is motivated by applications in Narrowband Internet of Things (NB-IoT). As outlined in LTE physical layer specifications [21], NB-IoT is deployed in one resource

Table 2.2: Parameters in NB-IoT

Parameter	Value
Maximum bandwidth	200 kHz (20 kHz is for Guard band)
Multiple access scheme	OFDM (downlink) and SC-FDMA (uplink)
Modulation	QPSK
Subcarrier spacing	15 kHz and 3.75 kHz (only available for uplink)

block (RB) of LTE, which has the bandwidth of 200 kHz (only 180 kHz is available for data transmission). This RB can either be one of the normal LTE's RB for carrying data, or in the LTE's guardband. Since NB-IoT is used for low-power low-rate applications, the highest modulation order is 4 (corresponding to QPSK). Using such small constellations ensures that good error performance can be obtained with low transmit powers. Furthermore, in addition to the subcarrier spacing of 15 kHz adopted from LTE, one can use single tone with 3.75 kHz spacing for uplink transmission. This is particularly useful in the cases when devices such as sensors send small packets of data to the base stations. Some important parameters in the physical layer of NB-IoT are summarized in Table 2.2, where SC-FDMA refers to Single-Carrier Frequency-Division Multiple Access.

3. Fast-OFDM with Index Modulation for NB-IoT

Published as [1]*:*

Nghia H. Nguyen, Brian Berscheid, and Ha H. Nguyen, "Fast-OFDM with Index Modulation for NB-IoT", *IEEE Communications Letters*, vol. 23, no. 7, pp. 1157-1160, July 2019.

In the previous chapter, the system model of OFDM with index modulation has been presented. It was also shown that two-stage signal detection methods are more practical than the optimal ML receiver. In this chapter, the combination of index modulation with fast-OFDM (a form of NFDM with $\alpha = 0.5$) is considered. The bit error probability of the two-stage detector is derived when one-dimension constellations are employed in the fast-OFDM system. Then, the use of modified constellations is proposed to minimize the BEP in this system, which eventually leads to better operating points in terms of spectral efficiency.

[1] Changes highlighted in blue has been made in this chapter to address comments from examination committee's members.

Fast-OFDM with Index Modulation for NB-IoT

Nghia H. Nguyen, Brian Berscheid, and Ha H. Nguyen

Abstract

In this paper, a hybrid orthogonal frequency-division multiplexing (OFDM)-based modulation technique for narrowband Internet of Things (NB-IoT) is introduced and analyzed. The technique combines fast-OFDM with index modulation in order to maximize bandwidth and power efficiency for IoT applications. The ideal number of active subcarriers to maximize spectral efficiency is derived. The one-dimensional constellation used in fast-OFDM is also optimized to enhance error performance of the proposed system. Numerical results indicate that the proposed system outperforms other OFDM systems based on index modulation in the relatively low signal-to-noise ratio (SNR) region, while it provides additional design options for trading off power efficiency and spectral efficiency in the higher SNR region.

Index terms

OFDM, Index Modulation, fast-OFDM, NB-IoT

3.1 Introduction

Narrowband Internet of Things (NB-IoT) has recently attracted a great deal of attention from the research community [22–24] and was standardized as a part of Long Term Evolution (LTE). It can be deployed using 200 kHz of LTE's in-use band (in-band mode) or LTE's guard band (guard-band mode), with the subcarrier spacing of either 15 kHz or 3.75 kHz. Future variations of NB-IoT must evolve together with the 5G mobile network to meet the requirements of massive machine-type communication networks in serving huge numbers of low-cost, power efficient devices. As a result, the available 200 kHz bandwidth must be utilized in an ultra-efficient way.

Orthogonal frequency-division multiplexing (OFDM) with index modulation (OFDM-IM) has been proposed and widely researched [20, 25, 26] in recent years as a technique en-

abling power and bandwidth efficient communications. It is now widely regarded as a favorable candidate for future communication standards. OFDM-IM allows a subset of available subcarriers to be active with the remainder left inactive. The pattern of active subcarriers is used to convey information (so-called index bits), in addition to the constellation bits which are conventionally modulated onto the active subcarriers.

Fast-OFDM [27] is a variation of OFDM which reduces the subcarrier spacing by a factor of two. This allows twice as many subcarriers to be placed within a fixed bandwidth as compared to conventional OFDM. Orthogonality among fast-OFDM subcarriers is still preserved if the constellation is restricted to one-dimensional modulation, such as amplitude-shift keying (ASK) [28]. Due to the restriction of one-dimensional modulation, fast-OFDM is best suited for low-rate applications, where low modulation orders are sufficient and preferable.

In this paper, we introduce a novel system as a very promising candidate for low-rate applications, such as NB-IoT. By combining index modulation with fast-OFDM, we show that advantageous trade-offs between spectral efficiency and energy efficiency can be obtained, especially for the low signal-to-noise ratio (SNR) region. To optimize the error performance in such a system we propose the use of properly-designed non-uniform ASK constellations. Numerical results demonstrate the preeminence of the proposed system in bandwidth efficiency at low SNRs.

3.2 System Model

Consider an OFDM system having N subcarriers in total. Neglecting the cyclic prefix for notational simplicity, the OFDM signal in the time domain can be expressed as

$$s(t) = \sum_{n=0}^{N-1} C_n \mathrm{e}^{\frac{j2\pi nt}{T}}, \tag{3.1}$$

where C_n denotes the symbol modulating the nth subcarrier, and T is the symbol duration. In an OFDM-IM system, of the N subcarriers only K subcarriers carry symbols drawn from a traditional constellation. The remaining $(N-K)$ are left inactive, i.e., $C_n = 0$. Within an OFDM-IM symbol, the positions of the active subcarriers create a unique combination which corresponds to a set of data bits, commonly referred to as index bits. The number of

index bits is equal to the floor of the base-2 logarithm of an "N choose K" operation.

Sampling the signal in (3.1) with the period of $\frac{T}{2N}$ generates a signal that occupies half of the bandwidth of the original OFDM-IM. As a result, one can place a second length-N OFDM-IM symbol within the original bandwidth. As such, the number of subcarriers in the resulting system is twice that of an ordinary OFDM-IM system [27]. We refer to this approach as fast-OFDM-IM and denote $\hat{N} = 2N$ as the total number of its subcarriers.

The total number of bits transmitted in one fast-OFDM-IM symbol can be calculated as

$$\lambda = \underbrace{\hat{K}\log_2 M}_{\lambda_1} + \underbrace{\left\lfloor \log_2 \begin{pmatrix} \hat{N} \\ \hat{K} \end{pmatrix} \right\rfloor}_{\lambda_2}. \tag{3.2}$$

In (3.2), M is the ASK modulation order, $\hat{K}$ is the number of active subcarriers in the fast-OFDM-IM system, λ_1 and λ_2 represent the number of constellation bits and the number of index bits, respectively.

3.3 Performance and Constellation Design

3.3.1 Number of Active Subcarriers

Given the system parameters $\{\hat{N}, M\}$, the value of $\hat{K}$ determines the system's bandwidth efficiency. In this section, we derive an expression for the optimal value of $\hat{K}$. First, due to the floor function in (3.2), the following inequality must hold

$$\lambda \leq \hat{K}\log_2 M + \log_2 \begin{pmatrix} \hat{N} \\ \hat{K} \end{pmatrix}. \tag{3.3}$$

Taking the first derivative with respect to $\hat{K}$, one obtains

$$\frac{d\lambda}{d\hat{K}} \leq \log_2 M + \frac{1}{\log 2}\left(H_{\hat{N}-\hat{K}} - H_{\hat{K}}\right), \tag{3.4}$$

where $H_{\hat{K}} = \sum_{k=1}^{\hat{K}} \frac{1}{k}$ is the $\hat{K}$th harmonic number. This parameter may be approximated as $H_{\hat{K}} \approx \gamma + \log\left(\hat{K}\right)$, where γ is the Euler constant. Substituting this into (3.4) and setting

$\frac{d\lambda}{d\hat{K}} = 0$, the optimum value of $\hat{K}$ is found to be

$$\hat{K} \approx \left\lfloor \frac{M\hat{N}}{M+1} \right\rfloor. \tag{3.5}$$

It is worth noting that the above analysis can be similarly applied to any ordinary OFDM-IM system with parameters $\{N, M\}$ to find the optimal number of active subcarriers K. In many IoT applications, due to transmit energy limitations, low constellation orders such as $M = 2$ and $M = 4$ are of particular interest. For these values of M, the optimum numbers of active subcarriers are approximately $\frac{2}{3}N$ and $\frac{4}{5}N$, respectively.

3.3.2 Detection and Performance Analysis

For the purpose of analyzing the detection performance, we assume, without loss of generality, all of the inactive subcarriers are assigned to the rearmost end of the spectrum. Thus, the length-$\hat{N}$ fast-OFDM-IM symbol in the frequency domain is denoted as

$$\mathbf{c} = [C_1, \ldots, C_{\hat{K}}, 0, \ldots, 0]^\top, \tag{3.6}$$

For an additive white Gaussian noise channel (AWGN), assuming perfect timing synchronization, the received signal can be expressed as

$$\mathbf{r} = \mathbf{c} + \mathbf{w} = [r_1, \ldots, r_{\hat{N}}]^\top, \tag{3.7}$$

where $\mathbf{w} \sim \mathcal{N}(\mathbf{0}, \sigma^2\mathbf{I})$ is a length-$\hat{N}$ Gaussian noise vector. Note that $\mathbf{r}$, $\mathbf{c}$ and $\mathbf{w}$ consist of real values due to the use of one-dimensional modulation. Also the variance of the noise component is commonly expressed in terms of the two-sided power spectral density of white Gaussian noise as $\sigma^2 = \frac{N_0}{2}$.

A straightforward detection approach is to find the magnitudes of the $\hat{N}$ symbols and then select the $\hat{K}$ largest magnitudes, similar to the approach in [14]. By doing so, the active subcarrier pattern is first detected to recover the index bits, then the $\hat{K}$ active subcarriers are further processed to recover the constellation bits. Let random variables X and Z represent the magnitudes of the received active subcarriers and inactive subcarriers, respectively. The cumulative distribution functions (cdf) and probability density functions (pdf) of these random variables are denoted as $F_X(x)$, $f_X(x)$, $F_Z(z)$ and $f_Z(z)$.

In a fast-OFDM-IM system using an ASK constellation, X and Z are the absolute values of Gaussian distributed random variables, and thus follow a mixture of folded-normal and half-normal distributions, respectively. In particular, the cdfs of X and Z are given as

$$F_X(x) = \frac{1}{M}\sum_{m=1}^{M}\left[1 - Q\left(\frac{x+\Delta_m}{\sigma}\right) - Q\left(\frac{x-\Delta_m}{\sigma}\right)\right], \tag{3.8}$$

where Δ_m is the distance from mth signal point in the M-ASK constellation to the origin, and

$$F_Z(x) = 1 - 2Q\left(\frac{x}{\sigma}\right). \tag{3.9}$$

Next, define $X_{\min}$ as the minimum value of X's among the $\hat{K}$ active subcarriers and $Z_{\max}$ the maximum value of Z's among $\hat{N} - \hat{K}$ inactive subcarriers. Their cdfs are given as [29]

$$F_{Z_{\max}}(x) = F_Z(x)^{\hat{N}-\hat{K}} \tag{3.10}$$

and

$$F_{X_{\min}}(x) = 1 - (1 - F_X(x))^{\hat{K}}. \tag{3.11}$$

As in the detection approach presented in [14], an error in detecting the index bits happens if $X_{\min} < Z_{\max}$. This error probability can be formulated as

$$P_{\text{idx}} = P(X_{\min} < Z_{\max}) = \int_0^\infty F_{X_{\min}}(x)\, f_{Z_{\max}}(x)\, dx \tag{3.12}$$

In [14], an optimized bit-to-subcarrier mapping method was proposed such that an error in detecting the active subcarrier pattern yields errors on the constellation bits corresponding to only two active subcarriers. Considering the use of such a mapping scheme, the bit error probability (BEP) of a fast-OFDM-IM system over an AWGN channel is calculated as

$$\begin{aligned} P_e = & \underbrace{P_{\text{idx}}\left(\frac{\lambda_2}{2\lambda} + \frac{\lambda_1}{\lambda}\left(\left(\frac{\hat{K}-2}{\hat{K}}\right)P_{\text{const}} + \frac{1}{\hat{K}}\right)\right)}_{P_{e,1}} \\ & + \underbrace{(1 - P_{\text{idx}})\frac{\lambda_2}{\lambda}P_{\text{const}}}_{P_{e,2}}. \end{aligned} \tag{3.13}$$

In (3.13) above, $P_{e,1}$ is equal to the BEP in the case that an incorrect index detection occurs, and $P_{e,2}$ is the BEP of constellation bit detection given correct index detection. In both terms, P_{const} is the BEP of the optimum detection of M-ASK. Denoting as E_s the average symbol energy of the conventional M-ASK constellation (i.e., with all M signal points equally spaced around the origin), this BEP is well approximated as [16]

$$P_{\text{const}} \approx \frac{2\,(M-1)}{M\log_2 M} Q\left(\sqrt{\frac{6}{M^2-1}\frac{E_s}{N_0}}\right). \tag{3.14}$$

3.3.3 Constellation Design

Fig. 3.1 plots the two terms in (3.13) over a range of the SNR per bit, E_b/N_0, where $N_0 = 2\sigma^2$ and $E_b = \frac{\hat{K}E_s}{\lambda}$. From Fig. 3.1, one observes that $P_e \approx P_{e,1}$ regardless of E_b/N_0. This implies that the index detection performance is the limiting factor in the overall BEP. To obtain the best overall performance, we propose to use modified M-ASK constellations, where the distribution of signal points is no longer uniform. For the particular case of $M = 4$ as illustrated in Fig. 3.2, $P_{e,1}$ can be diminished by moving the smallest non-zero signal further from the origin. As a consequence, the minimum distance among non-zero signals becomes smaller yielding worse symbol detection performance (i.e., higher $P_{e,2}$) for active subcarriers. However, given the initial dominance of $P_{e,1}$, the net effect is to reduce the overall BEP.

Referring to Fig. 3.2, let Δ_1 be the distance between the two non-zero points closet to the origin, and Δ_2 be the distance between the other pairs of non-zero points These two parameters may be combined into a single ratio $\alpha = \frac{\Delta_1}{\Delta_2}$ for optimization. Our objective is to minimize the total BEP.

First, the BEP of the modified constellation is derived using the total probability theorem as

$$P_{\text{const}} \approx \frac{Q\left(\frac{\Delta_2}{2\sigma}\right) + \frac{2}{M}Q\left(\frac{\alpha\Delta_2}{2\sigma}\right)}{\log_2 M}. \tag{3.15}$$

The distribution of $F_Z(z)$ is unaffected by Δ_1 and Δ_2. As a result of using the modified

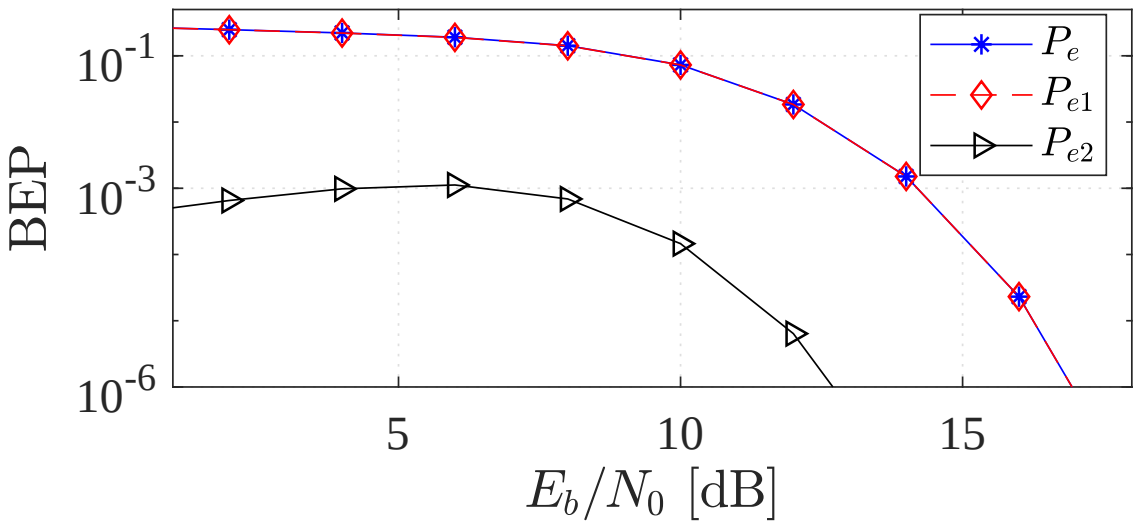

Figure 3.1: Comparison of error components.

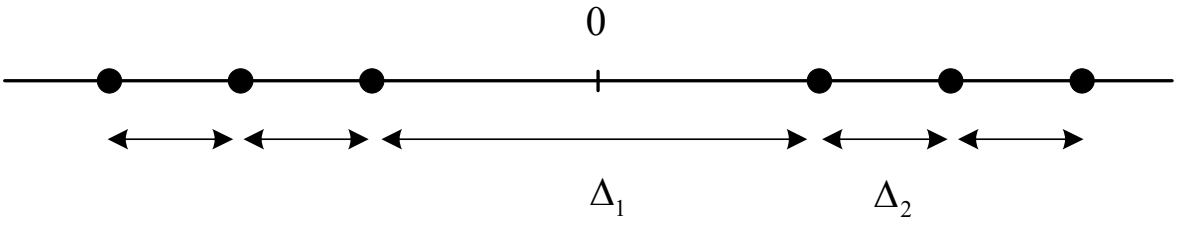

Figure 3.2: Modified ASK constellation.

constellation, $F_X(x)$ becomes

$$F_X(x) = 1 - \frac{2}{M}\sum_{i=0}^{\frac{M}{2}-1} Q\left(\frac{x + \left(\frac{\alpha}{2} + i\right)\Delta_2}{\sigma}\right) + Q\left(\frac{x - \left(\frac{\alpha}{2} + i\right)\Delta_2}{\sigma}\right). \tag{3.16}$$

Substituting (3.16) into (3.11) gives

$$F_{X_{\min}}(x) = 1 - \left(\frac{2}{M}\sum_{i=0}^{\frac{M}{2}-1} Q\left(\frac{x + \left(\frac{\alpha}{2} + i\right)\Delta_2}{\sigma}\right) + Q\left(\frac{x - \left(\frac{\alpha}{2} + i\right)\Delta_2}{\sigma}\right)\right)^{\hat{K}}. \tag{3.17}$$

Combining (3.9)–(3.13) and (3.17), one obtains P_e as a function of α as in (3.18).

$$P_e = P_{\text{idx}}\left(\frac{\lambda_2}{2\lambda} + \frac{\lambda_1}{\lambda}\left(\left(\frac{\hat{K}-2}{\hat{K}}\right)\frac{Q\left(\frac{\Delta_2}{2\sigma}\right) + \frac{2}{M}Q\left(\frac{\alpha\Delta_2}{2\sigma}\right)}{\log_2 M} + \frac{1}{\hat{K}}\right)\right) + (1 - P_{\text{idx}})\frac{\lambda_2}{\lambda}\frac{Q\left(\frac{\Delta_2}{2\sigma}\right) + \frac{2}{M}Q\left(\frac{\alpha\Delta_2}{2\sigma}\right)}{\log_2 M}. \tag{3.18}$$

An iterative search [2] can then be easily conducted to find the value of α which minimizes P_e. The results are reported in the next section.

3.4 Numerical Results

3.4.1 Optimum Bit Rate and Error Performance

We consider an OFDM-IM system with $N = 12$ and a fast-OFDM-IM system with $\hat{N} = 24$ corresponding to the 200 kHz bandwidth available in NB-IoT. The maximum number of transmitted bits per symbol duration in each system is shown in Table 3.1 for various modulation orders. One can see a very close match between the approximate values obtained from (3.5) and the exact optimum values indicated by arrows in Fig. 3.3. A slight mismatch occurs due to the approximation's inequality, yielding an error of one bit between

[2] For each value of Δ_2/σ, the search runs over a range of α to obtain the smallest value of P_e using algorithm such as golden-section search.

Table 3.1: Rate comparison in a NB-IoT channel.

	OFDM-IM		Fast-OFDM-IM		
M	K (exact)	λ	$\hat{K}$ approx by (3.5)	$\hat{K}$ (exact)	λ
2	7	16	16	15	35
4	10	25	19	18	53
8	10	36	21	22	73
16	12	47	22	22	96

the approximate and exact values. This difference is negligible compared to total numbers of transmitted bits, justifying the usefulness of the approximation. More importantly, fast-OFDM-IM has a superior bit rate as it delivers approximately twice as many bits as OFDM-IM does (assuming equal modulation orders).

Next, we compare the error performance of four OFDM-IM systems: OFDM-IM with phase-shift keying (PSK), OFDM-IM with quadrature-amplitude modulation (QAM), fast-OFDM-IM with conventional ASK and fast-OFDM-IM with the optimum ASK developed in Section 3.3.3. System parameters are selected according to Table 3.1. Note that the numbers of total subcarriers and active subcarriers in fast-OFDM-IM are $\hat{N}$ and $\hat{K}$, while those in OFDM-IM are denoted as N and K. At each value of E_b/N_0, the optimal ratio α for the optimum ASK system was determined by a computer search. Note that the optimal α values for various SNRs could be precomputed offline.

Fig. 3.4 compares the four systems in terms of error rate. When $M = 2$, the error performance of all systems are equivalent since antipodal signaling is employed. When $M = 4$, OFDM-IM systems with PSK and QAM outperform fast-OFDM-IM systems with optimum ASK and conventional ASK by 5 dB and 7 dB, respectively. It is important to point out that the power gains of OFDM-IM over fast-OFDM-IM are compromised by the much lower rate as demonstrated in detail in the next subsection. On the other hand, an important observation from Fig. 3.4 is that, within the fast-OFDM-IM approach, using the optimum ASK provides a gain of about 2 to 2.5 dB compared to using the conventional

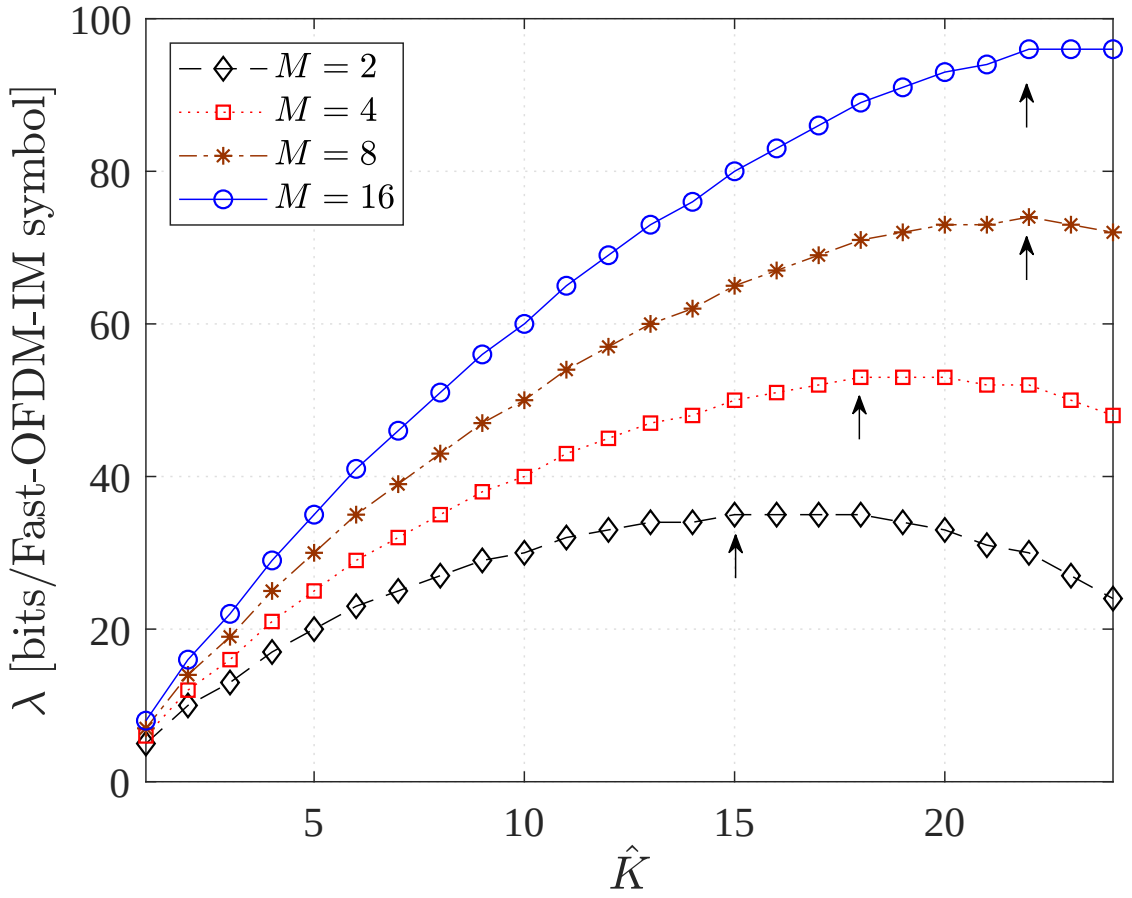

Figure 3.3: Optimum choices of active subcarriers.

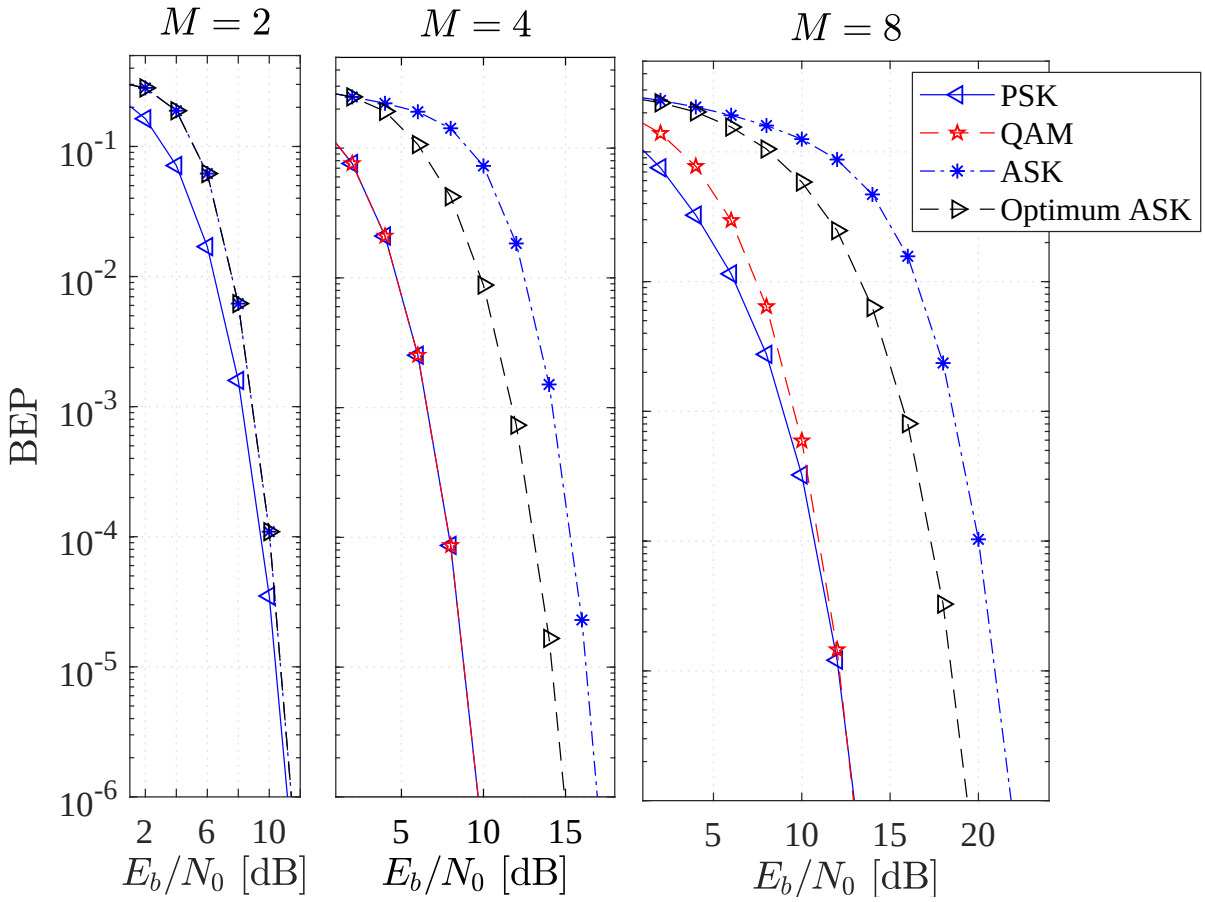

Figure 3.4: Comparison of BEP.

ASK for both cases of $M = 4$ and $M = 8$. This clearly demonstrates the superiority of our optimized ASK constellation compared to the conventional ASK.

3.4.2 Spectral Efficiency

Fig. 3.5 compares the spectral efficiency and power efficiency of the four systems at BEP of 10^{-6}. It can be seen that for $E_b/N_0 < 13$dB, fast-OFDM-IM with $M = 2$ achieves approximately 40% greater spectral efficiency than conventional OFDM-IM (approximately 2.9 vs 2.1 bits/s/Hz). Since low-SNR performance is of paramount importance in IoT applications, fast-OFDM-IM is an attractive option. At higher SNRs, due to the discrete nature of M, conventional QAM-based OFDM-IM allows a limited number of operating points within the power-bandwidth plane. As shown in Fig. 3.5, as M is increased, fast-OFDM-IM provides additional operating points along the same curve, allowing system designers more granularity when trading off power and spectral efficiency. Thus, a system supporting both fast-OFDM-IM and conventional OFDM-IM could allow improved spectral efficiency over a variety of operating conditions.

3.5 Conclusion

In this paper, a hybrid index modulation-based fast-OFDM system that is well suited for NB-IoT applications has been introduced and analyzed. An expression for the optimum number of active subcarriers is derived and a modified ASK constellation which is shown to yield a 2 dB improvement over conventional ASK is proposed. Numerical results show that the proposed system is particularly favorable for low-power applications with SNR per bit of around 10–15 dB due to its spectral efficiency. Future studies could investigate hardware-efficient implementation structures for fast-OFDM-IM, as well as the benefit of jointly optimizing the number of active subcarriers and the ASK constellation.

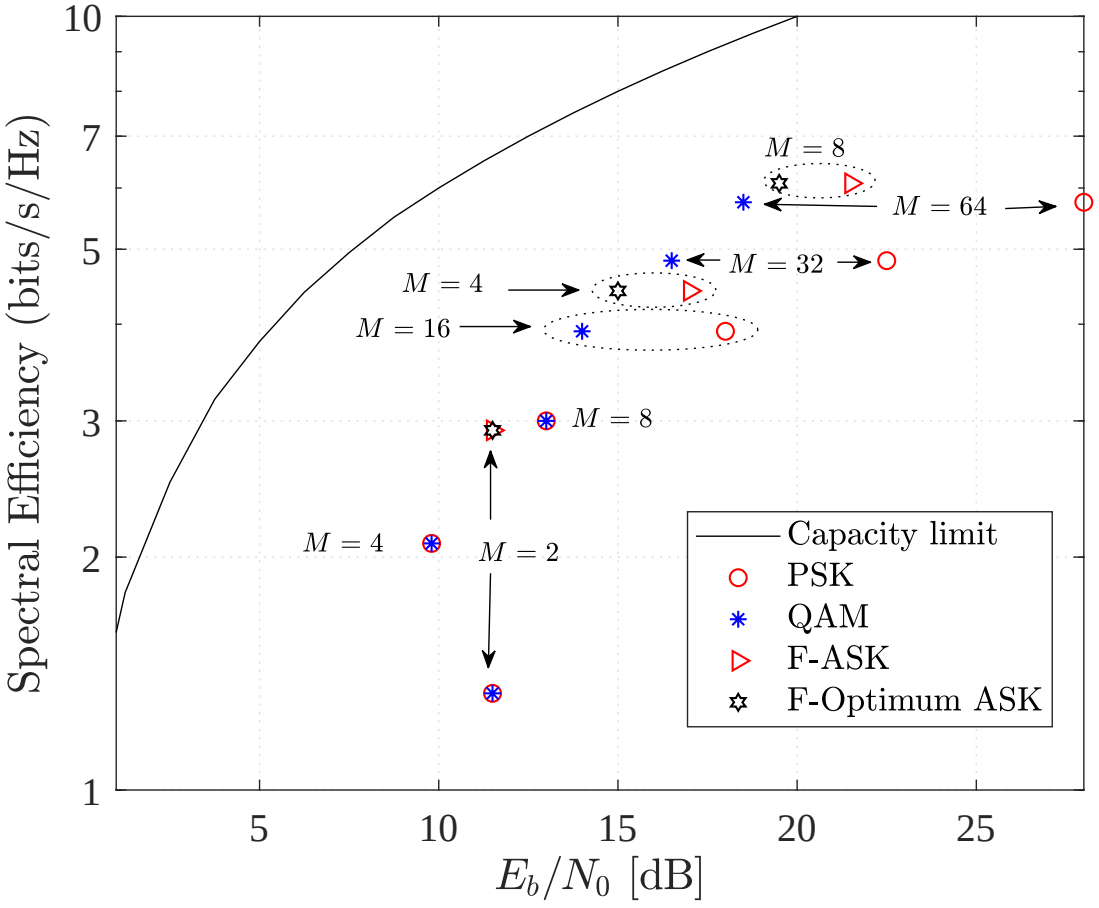

Figure 3.5: Spectral efficiency vs. E_b/N_0 with $N = 12$ or $\hat{N} = 24$.

4. SVD-Based Design for Non-Orthogonal Frequency Division Multiplexing

Published as:

Nghia H. Nguyen, Ha H. Nguyen, and Brian Berscheid, "SVD-Based Design for Non-Orthogonal Frequency Division Multiplexing", *IEEE Communications Letters*, to appear.

In Chapter 2, the conventional design of NFDM systems has been presented. The detection method and its drawback were also discussed, highlighting the disadvantage of NFDM compared to OFDM systems in terms of error performance. Being motivated by this fact, this chapter presents a novel design for NFDM systems which is able to completely suppress ICI without the need of an expensive receiver. Theoretical and simulation results show that the proposed NFDM systems achieve equivalent error rate as that of OFDM systems over AWGN channels. Furthermore, a suitable spectrum shaping method to control the power spectrum density of the proposed system is presented. Extensive experiments in various scenarios show that the proposed NFDM systems are more spectrally-efficient than the conventional OFDM under certain conditions.

SVD-Based Design for Non-Orthogonal Frequency Division Multiplexing

Nghia H. Nguyen, Ha H. Nguyen, and Brian Berscheid

Abstract

Conventional non-orthogonal frequency division multiplexing (NFDM) suffers from inter-channel interference (ICI) due to the loss of orthogonality among subcarriers. The ICI significantly degrades system performance and complicates the design of the receiver. In this paper we propose a novel NFDM design based on singular-value decomposition of the modified Fourier matrix, which is able to completely eliminate ICI over an AWGN channel, while enjoying a simple transceiver structure. We also introduce a novel cyclic prefix extension scheme for the proposed NFDM design which is shown to reduce out-of-band emissions as compared to the traditional method of NFDM cyclic prefix extension. The spectral efficiency of our proposed technique is investigated and carefully compared to that of OFDM. The results show that the proposed scheme achieves up to 23% higher bandwidth efficiency than OFDM while meeting the same target bit error rate performance.

Index terms

NFDM, OFDM, spectral efficiency, precoding

4.1 Introduction

Orthogonal frequency-division multiplexing (OFDM) is a well-established technique and adopted in various communication standards, such as IEEE 802.11 and Long Term Evolution (LTE) mobile networks. A key feature of OFDM is that its subchannels are orthogonally overlapped in the frequency domain, leading to an efficient use of the system's bandwidth. While having orthogonal subchannels (or equivalently orthogonal subcarriers) is a desirable property because it allows simple and parallel detection of information symbols sent over all the subcarriers, it is not necessary the best design choice when considering other performance metrics, such as the system's spectral efficiency.

As a matter of fact, the dominance of OFDM is being challenged, as future communication networks require increasingly efficient ways to utilize a limited bandwidth. Applications such as narrow-band Internet of Things (NB-IoT) and LTE-M1 are given just a small amount of bandwidth (particularly, 180 kHz for NB-IoT and 1.4 MHz for LTE-M1), but are designed to connect a massive number of low-power, low-rate devices. Such application scenarios are currently motivating significant research into alternatives to OFDM with the main goal of improving spectral efficiency.

Non-orthogonal frequency-division multiplexing (NFDM or NOFDM) or spectrally-efficient FDM (SEFDM) [30] is an alternative to OFDM. NFDM packs subcarriers more tightly than OFDM, yielding a smaller bandwidth while maintaining a similar bit rate[1], increasing spectral efficiency. However, a drawback of NFDM is the inter-channel interference (ICI) caused by the loss of orthogonality among subchannels [9]. The ICI, if not dealt with properly, degrades receiver performance, reducing the advantage of higher spectral efficiency.

ICI cancellation techniques for NFDM have been investigated in the literature. In [31], the authors proposed a method to self-cancel ICI by transmitting a single NFDM symbol and its image in two consecutive time slots. At the receiver, adding the two components yields an ICI-free received symbol. However, this scheme only applies when the NFDM subcarrier spacing is half that of OFDM. Furthermore, this approach doubles the time required to send one data symbol. Ultimately, the spectral efficiency of such a system is equivalent to that of OFDM. In [32] the authors apply a truncated singular value decomposition (SVD) to reduce the complexity of the conventional receiver. More recently, the authors in [33] investigated an iterative equalizer for ICI compensation. However, the results show that a greater bandwidth reduction results in poorer error performance. In addition, in order to recover each NFDM symbol, the iterative procedure is performed on each data point in the received constellation, which is much more computationally expensive than the simple one-tap equalizer used in OFDM. Another approach to handle ICI is to precode the signal at the transmitter. In [34], a precoding matrix derived from the correlation matrix is employed. However, this technique

[1] Alternatively, for the same bandwidth consumed by OFDM, one can pack a larger number of subcarriers (or subchannels).

suffers from noise amplification and severe performance degradation.

An important aspect of NFDM that has not been well studied in the literature is its power spectral density (PSD). Due to the loss of periodicity of the time-domain NFDM symbol, the conventional cyclic prefix or zero padding approaches for an NFDM system discussed in [35] cause discontinuities inside the NFDM symbol. Such discontinuities result in unfavorable transmit PSDs and limit the applicability of conventional methods of controlling the PSD of OFDM signals to NFDM.

In this paper we present a novel transceiver design for an NFDM system. The proposed scheme is capable of eliminating ICI completely through the use of SVD-based precoding in the transmitter and a linear detector in the receiver. The complexity of the proposed scheme is modest, while its error performance is the same as that of a single-carrier system. Furthermore, a practical implementation of the design is introduced that incorporates a novel approach to cyclic extension for controlling the PSD of the transmitted signal. Finally, the paper compares the error performance between NFDM and the state-of-the-art SEFDM with zero padding (ZP-SEFDM) in [35], as well as the spectral efficiency of the proposed NFDM system to that of OFDM system.

4.2 System Design

4.2.1 Conventional NFDM

Let N be the number of (non-orthogonal) subcarriers and denote the vector of constellation symbols as $\mathbf{s} = [s_1, \ldots, s_N]^\top$, where the symbol s_n belongs to a two-dimensional constellation (such as PSK or QAM) with an average symbol energy of $E\{\|s_n\|^2\} = E_s$. The expression for the discrete-time samples of the NFDM signal is

$$y_k = \frac{1}{\sqrt{N}} \sum_{n=1}^{N} s_n \exp\left(\frac{j2\pi\alpha(n-1)(k-1)}{N}\right), \; k = 1, \ldots, N, \tag{4.1}$$

where α is the compressing factor of the subcarrier spacing. For example, $\alpha = 0.5$ means that the subcarrier spacing in NFDM is half of that in OFDM. By defining $\mathbf{y} = [y_1, \ldots, y_N]^\top$ and $\mathbf{F}$ as the "modified" inverse Fourier matrix whose (k,n)th element is $f_{n,k} = \frac{1}{\sqrt{N}} \exp\left(\frac{j2\pi(n-1)(k-1)\alpha}{N}\right)$, the time samples can be equivalently obtained as $\mathbf{y} = \mathbf{F}\mathbf{s}$.

Considering an AWGN channel, the received signal samples are $\mathbf{r} = [r_1, \ldots, r_N]^\top = \mathbf{y}+\mathbf{w}$, where $\mathbf{w} = [w_1, \ldots, w_N]^\top$ is a vector of independent zero-mean complex Gaussian random variables with variance N_0. The received signal vector $\mathbf{r}$ is then multiplied with $\mathbf{F}^{\mathrm{H}}$, i.e., the modified Fourier matrix, in order to recover the information symbol in each subchannel:

$$\mathbf{F}^{\mathrm{H}}\mathbf{y} = \mathbf{F}^{\mathrm{H}}\mathbf{F}\mathbf{s} + \mathbf{F}^{\mathrm{H}}\mathbf{w} = \mathbf{C}\mathbf{s} + \mathbf{F}^{\mathrm{H}}\mathbf{w}, \tag{4.2}$$

where $\mathbf{C} = \mathbf{F}^{\mathrm{H}}\mathbf{F}$ is a matrix representing correlations among subcarriers. Note that in OFDM, $\alpha = 1$ and $\mathbf{F}^{\mathrm{H}}$ and $\mathbf{F}$ are standard Fourier and inverse Fourier matrices, respectively. This makes $\mathbf{C} = \mathbf{I}$, leading to N non-interfering parallel channels, a well-known property of OFDM. In contrast, $\alpha < 1$ in NFDM, which makes $\mathbf{C}$ not an identity matrix, hence there is interference injected from one subcarrier to its neighbours. The amount of interference becomes more severe as α decreases, ultimately limiting the extent to which the bandwidth of an NFDM signal can be reduced (when N is fixed).

4.2.2 Proposed Design

In this section, we propose a scheme that can suppress ICI in an NFDM system with an arbitrary compression factor α. First, the nth symbol in vector $\mathbf{s}$ is scaled by g_n. By defining a diagonal matrix $\mathbf{G} = \mathrm{diag}(g_1, \ldots, g_N)$, the scaled symbol vector is $\mathbf{s}_g = \mathbf{G}\mathbf{s}$. The choice of scaling factors $\{g_n\}$ is an important design decision and will be discussed in more detail in subsequent sections.

The symbol vector is then precoded as $\mathbf{s}_v = \mathbf{V}\mathbf{s}_g$, where $\mathbf{V}$ is obtained from the SVD of the modified inverse Fourier matrix as $\mathbf{F} = \mathbf{U}\mathbf{D}\mathbf{V}^{\mathrm{H}}$. Matrices $\mathbf{U}$ and $\mathbf{V}$ are unitary, and $\mathbf{D} = \mathrm{diag}(d_1, \ldots, d_N)$ is a diagonal matrix whose elements are singular values of $\mathbf{F}$. Next, the precoded vector is processed with matrix $\mathbf{F}$ (as in the conventional NFDM) to produce a vector of time samples $\mathbf{y} = \mathbf{F}\mathbf{V}\mathbf{s}_g = \mathbf{U}\mathbf{D}\mathbf{G}\mathbf{s}$. The average symbol energy of precoded NFDM is:

$$\begin{aligned}\frac{1}{N}E\left\{\mathbf{y}^{\mathrm{H}}\mathbf{y}\right\} &= \frac{1}{N}E\left\{\mathbf{s}^{\mathrm{H}}\mathbf{G}^{\mathrm{H}}\mathbf{D}^{\mathrm{H}}\mathbf{U}^{\mathrm{H}}\mathbf{U}\mathbf{D}\mathbf{G}\mathbf{s}\right\} \\ &= \frac{1}{N}\sum_{n=1}^{N} g_n^2 d_n^2 E\left\{\|s_n\|^2\right\} = \left(\frac{1}{N}\sum_{n=1}^{N} g_n^2 d_n^2\right) E_s. \end{aligned} \tag{4.3}$$

Thus, in order to maintain the same average symbol energy of E_s as in the conventional NFDM, the gains $\{g_n\}$ should be chosen such that $\frac{1}{N}\sum_{n=1}^{N} g_n^2 d_n^2 = 1$. As long as all the singular values of $\mathbf{F}$ are non zero, we can simply set $g_n = 1/d_n$ to meet this requirement. In general, both the values of N and α strongly influence the values of $\{d_n\}$ as well as the PSD of the transmitted NFDM signal. For example, if α is small, many singular values of $\mathbf{F}$ are very small, which makes setting $g_n = 1/d_n$ impractical. As such, practical choices of $\{g_n\}$ would need to take into account the values of $\{d_n\}$ as well as the PSD of the NFDM signal. This will be discussed in more detail in Section 4.3.

The received signal over an AWGN channel is then given as $\mathbf{r} = \mathbf{UDGs} + \mathbf{w}$, where $\mathbf{w} \sim \mathcal{CN}(0, N_0\mathbf{I})$. At the receiver, a decoding matrix $\mathbf{U}^{\mathrm{H}}$ is first applied to $\mathbf{r}$ to produce:

$$\hat{\mathbf{s}} = \mathbf{U}^{\mathrm{H}}\mathbf{r} = \mathbf{DGs} + \tilde{\mathbf{w}}, \tag{4.4}$$

where $\tilde{\mathbf{w}} = \mathbf{U}^{\mathrm{H}}\mathbf{w} \sim \mathcal{CN}(0, N_0\mathbf{I})$, i.e., having the same statistics as $\mathbf{w}$. Since the matrix $\mathbf{DG}$ is diagonal, the equivalent system is that of a set of parallel ICI-free channels:

$$\hat{s}_n = d_n g_n s_n + \tilde{w}_n, \quad n = 1, \ldots, N. \tag{4.5}$$

The expression in (4.5) indicates that, as long as all the singular values $\{d_n\}$ are non zero, it is theoretically possible to set $g_n = 1/d_n$ so that all N channels enjoy the same signal-to-noise ratio (SNR) of E_s/N_0, which is exactly the same as that of OFDM system. Since an NFDM signal occupies less bandwidth than OFDM (thanks to a tighter packing of subchannels), this result implies that a higher spectral efficiency is achieved by NFDM than OFDM. While such a conclusion is plausible, care must be taken in making spectral comparisons between NFDM and OFDM. As will be seen in the next section, a caveat with the NFDM signal is that its PSD is very poor when α is small, limiting the true spectral efficiency benefit of NFDM.

4.2.3 Complexity

In terms of computational complexity, the conventional OFDM system requires $\mathcal{O}(N\log(N))$ operations for performing IFFT and FFT. The cost of the proposed NFDM design is dominated by the precoding and decoding steps in the transmitter and receiver, respectively.

These operations multiply an N-element vector by an $N \times N$ matrix, yielding a complexity of $\mathcal{O}(N^2)$. Therefore, the implementation of the proposed NFDM is more expensive than conventional OFDM. Nevertheless, the increased complexity of the proposed NFDM could be well justified by its superior spectral efficiency, as discussed further in the simulation results section.

4.3 NFDM with Cyclic Extension over Multipath Channels

Similar to OFDM, NFDM experiences discontinuities between consecutive symbols in the time domain. This leads to out-of-band (OOB) radiation, potentially causing interference in adjacent frequency bands. It is worth noting that the NFDM signal as conventionally generated does not have periodicity in the time domain. Therefore, the conventional method of performing CP extension on NFDM symbols by prepending the last few samples to the front of the symbol as described in [35] (essentially the same method used in conventional OFDM) suffers from time-domain discontinuities not only at the symbol transition but within each symbol itself. Such time-domain discontinuities also happen with the use of zero padding (ZP) in NFDM. The time-domain discontinuities severely limit the effectiveness of windowing for controlling OOB emissions since discontinuities occur inside the flat portion of the window.

In this section, we introduce a work-around solution for this problem. The main idea is to construct prefixed NFDM symbols such that the transmit waveform is continuous within each individual symbol. The proposed system, which shall be referred to as CP-NFDM, is presented in Fig. 4.1.

It is pointed out that the NFDM transmitter in Fig. 4.1 does not perform a multiplication with the modified Fourier matrix $\mathbf{F}$, whose complexity is about $\mathcal{O}(N^2)$. Instead, the implementation involves zero padding the precoded vector and performing size-$\frac{N}{\alpha}$ IFFT[2], where the $\frac{N}{\alpha} \times \frac{N}{\alpha}$ inverse Fourier matrix is denoted as $\mathbf{F}'$. The latter implementation provides an identical result, but with a lower complexity of $\mathcal{O}(N \log(N))$ [28]. Specifically, the length-N

[2]It is assumed that α is selected so that $\frac{N}{\alpha}$ is an integer.

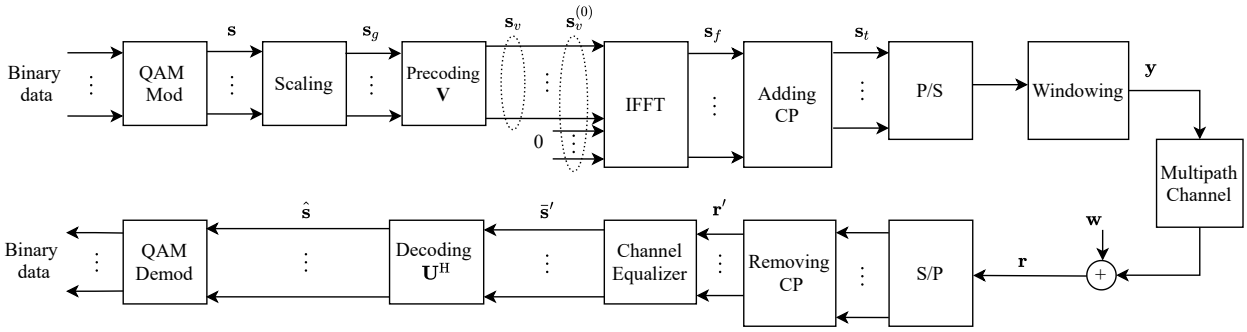

Figure 4.1: Implementation of the proposed CP-NFDM.

precoded signal $\mathbf{s}_v$ is first zero padded to become a length-$\frac{N}{\alpha}$ vector $\mathbf{s}_v^{(0)}$. This zero-padded vector enters the IFFT block to produce the signal vector:

$$\mathbf{s}_f = \mathbf{F}'\mathbf{s}_v^{(0)}. \tag{4.6}$$

The signal vector $\mathbf{s}_t$ contains $(N + L_1 + L_2)$ transmitted time samples, which are obtained from $\mathbf{s}_f$ as

$$\mathbf{s}_t = \begin{bmatrix} \mathbf{s}_f(N/\alpha - L_1 + 1 : N/\alpha) \\ \mathbf{s}_f(1 : N) \\ \mathbf{s}_f(N + 1 : N + L_2) \end{bmatrix}, \tag{4.7}$$

where L_1 and L_2 are prefix and postfix lengths, respectively. In essence, $\mathbf{s}_t$ is formed by concatenating the last L_1 and the first $N + L_2$ samples of $\mathbf{s}_f$. After this process, one observes a perfect continuity of $\mathbf{s}_t$ in the time domain, which is not the case with the conventional CP method.

Common approaches to control the PSD of OFDM signals include filtering and windowing [36, 37]. In this paper, we apply a raised cosine window to create smooth transitions from symbol to symbol. The windowing function is symmetric at the center $c = \frac{N+L_1+L_2}{2}$ and the right half is defined as $g[n + c] = 1$ with $0 \leq n \leq c - L_2 - 1$ and

$$g[n + c] = \frac{1}{2}\left(1 - \sin\left(\frac{\pi}{L_2}\left(n - \frac{N + L_1 - 1}{2}\right)\right)\right)$$

with $c - L_2 \leq n \leq c - 1$. Before transmitting, two consecutive NFDM symbols are overlapped, namely the last L_2 samples of the current symbol and the first L_2 samples of the next symbol are summed. The transmitted NFDM symbol thus has a length of $N + L_1$ and is denoted

as $\mathbf{y}$ in Fig. 4.1. It can be further represented as $\mathbf{y} = [\mathbf{y}_{\text{cp}}, \mathbf{y}']^{\text{T}}$, where $\mathbf{y}_{\text{cp}}$ is the length-L_1 cyclic prefix portion and $\mathbf{y}'$ is the length-N desired signal portion.

Consider a multipath fading channel, whose channel impulse response (CIR) is defined by a length-μ vector $\mathbf{h} = [h_1, \ldots, h_\mu]$. Then, the received signal $\mathbf{r}$ is obtained as

$$\mathbf{r} = \begin{bmatrix} \mathbf{r}_{\text{cp}} \\ \mathbf{r}' \end{bmatrix} = \mathbf{h} * \mathbf{y} + \mathbf{w} = \mathbf{H}\mathbf{y} + \mathbf{w}, \tag{4.8}$$

where $*$ denotes the convolution operation and $\mathbf{H}$ is in the form of a general Toeplitz matrix, whose first row and first column are $[h_1, 0, \ldots, 0]$ and $[h_1, \ldots, h_{\mu-1}, 0, \ldots, 0]^{\text{T}}$, respectively.

The multipath effect is eliminated by removing the CP segment $\mathbf{r}_{\text{cp}}$, leaving the desired signal $\mathbf{r}' = \mathbf{H}_1\mathbf{y} + \mathbf{w}'$, where $\mathbf{H}_1$ is the lower part of $\mathbf{H}$ with size $(N) \times (N + L_1)$. Then, $\mathbf{r}'$ is equalized based on the least square solution to obtain $\mathbf{s}' = \mathbf{H}_1^{\dagger}\mathbf{r}'$, where $\mathbf{H}_1^{\dagger}$ is the pseudo-inverse of $\mathbf{H}_1$. The desired portion of the equalized signal is then extracted and denoted as $\bar{\mathbf{s}}'$. Finally, the recovered signal before symbol demodulation is obtained as

$$\hat{\mathbf{s}} = \mathbf{U}^{\text{H}}\bar{\mathbf{s}}' \tag{4.9}$$

The analysis presented in Section 4.2.2 (for an "idealized" NFDM system that does not take into account discontinuities in the transmitted signal and hence does not implement CP extension and windowing) suggests choosing the gains as $g_n = 1/d_n$ if $d_n \neq 0$. However, if the proposed CP is used, it can be shown that the power in the prefix portion of the CP-NFDM signal increases as the gain factors increase. Furthermore, a wide range of g_n values may pose implementation challenges due to significant dynamic range requirements within the transmitter's precoding and IFFT blocks. For these reasons, it is undesirable to have large g_n values to compensate for small d_n values. Optimization of the gain values $\{g_n\}$ to make a good tradeoff between simplifying hardware implementation and maximizing the system's capacity is an interesting area for further investigation.

In the following sections, we follow the following heuristic rule for choosing the g_n values. Any subchannel for which $d_n \geq 1$ is used to carry data with its scaling factor set to $g_n = 1/d_n$, and any subchannel for which $d_n < 1$ is disabled (i.e., by setting $g_n = 0$). As a result of this approach, the effective number of active channels is reduced to $N_a \leq N$.

4.4 Experimental Bandwidth Measurements

In this section, we present the power spectral measurement results of NFDM and compare to that of OFDM. For NFDM, we investigate the following compressing factor values for $\alpha = \{0.1, 0.2, 0.5, 0.8\}$. Other parameters are: the total number of subcarriers $N = 256$, prefix length $L_1 = 20$ and postfix length $L_2 = 20$. The number of active subcarriers in OFDM is always N, whereas it is N_a in NFDM which is dependent on α through the distribution of d_n values.

With those parameters, signal bursts of 1000 symbols were generated in MATLAB and sent to a signal generator (Keysight N5182B). The signal generator then interpolates the signal at a sampling rate $F_s = 10^7$ samples per second and up-converts to a carrier frequency of $f_c = 2.4$ GHz. The output of the signal generator is connected to a spectrum analyzer (Keysight N9030A) via a coaxial cable. These steps were repeated for each measurement.

Fig. 4.2 compares the spectra of five systems: (i) CP-OFDM ($\alpha = 1$) without windowing, (ii) CP-OFDM with windowing, (iii) proposed NFDM ($\alpha = 0.5$) with conventional CP extension, (iv) proposed CP-NFDM without windowing, and (v) proposed CP-NFDM with windowing. As can be seen, the proposed CP extension method works very well with NFDM signals in terms of OOB suppression. When CP is added in the traditional way, the spectrum decays slowly and produces significant OOB emissions (see trace C). Meanwhile, using the suggested CP extension technique without windowing yields a much more localized spectrum (trace A) although the OOB leakage is still a bit more than the conventional CP-OFDM (the yellow line). However, when the windowing function is employed for both NFDM (trace B) and OFDM (cyan line), their OOB spectra have similar shapes.

To exactly measure the bandwidth, $\frac{P'}{P}$ is defined as the ratio of signal power captured in bandwidth B' to the total signal power. Table 4.1 presents the measured NFDM bandwidths of different combinations of $\{\frac{P'}{P}, \alpha\}$. From the table, we can infer that, for example, 90% of the signal power of NFDM with $\alpha = 0.5$ is contained in a bandwidth $B' = 4.3$ MHz.

Table 4.1: Measured NFDM bandwidth (in MHz).

α \ $\frac{P'}{P}$	90%	95%	98%
1	9	9.5	9.8
0.8	7.25	7.6	7.9
0.5	4.3	4.7	4.9
0.2	1.4	1.7	1.9
0.1	0.95	1.1	1.28

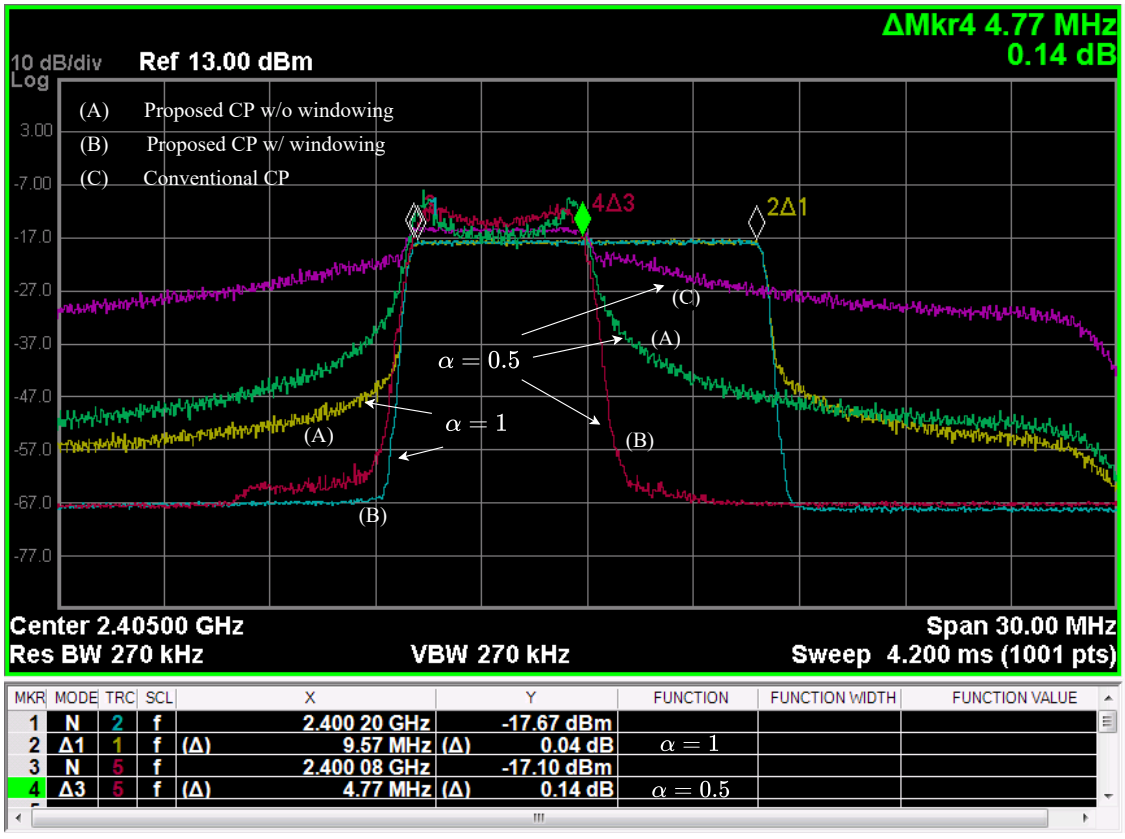

Figure 4.2: Spectrum comparison

4.5 Simulation Results

4.5.1 Bit Error Rate Performance

This section compares the bit error rate (BER) performance of three systems: OFDM, proposed NFDM design, and the state-of-the-art ZP-SEFDM using a sphere decoder detector in [35]. The structure of ZP-SEFDM is very similar to that of OFDM but with the use of the modified Fourier matrix instead of the conventional Fourier transform as in OFDM. Since no precoding is performed in ZP-SEFDM, ICI exists and a sphere decoder is used to obtain the near-optimal BER performance. The BER performance comparison is presented in Fig. 4.3 for both AWGN and multipath fading channels and with QPSK constellation. For the multipath channel, the same tapped delay line type-D (TDL-D) channel model as in [35] is adopted. Note that OFDM and NFDM are equipped with cyclic extension as in 4.3, while SEFDM is implemented with zero padding, which is shown to be better than implementing cyclic prefix [35]. To focus on the transmission and detection principles of different systems, results are obtained with perfect channel state information.

The results in Fig. 4.3 show that, over an AWGN channel, NFDM performs exactly the same as OFDM regardless of the compressing factor α, which agrees with the theoretical analysis in (4.5). On the other hand, the BER performance of SEFDM depends strongly on the compressing factor, namely a higher compression factor leads to higher BER. This is expected for SEFDM design since ICI power gets larger for a higher compression factor and degrades the performance of the sphere decoder. Clearly, our proposed NFDM design outperforms SEFDM. For example, NFDM requires the SNR per bit of 6.8 dB to achieve a BER of 10^{-3} while SEFDM with $\alpha = 0.8$ and $\alpha = 0.5$ needs 7.5 dB and 9.0 dB, respectively.

Different from the case of an AWGN channel, the BER performance of the proposed CP-NFDM over the TDL-D channel is affected by compressing factor α. This can be explained by examining Eq. (4.9) where the noise is essentially enhanced by the combined equalization/decoding operation, namely $\mathbf{U}^{\mathrm{H}}\mathbf{H}_1^{\dagger}$, which is dependent on α. Nevertheless, the proposed CP-NFDM still outperforms ZP-SEFDM. For example, to obtain a BER of 10^{-3}, CP-NFDM with $\alpha = 0.5$ requires 8.7 dB while ZP-SEFDM with $\alpha = 0.5$ needs an extra 5.0

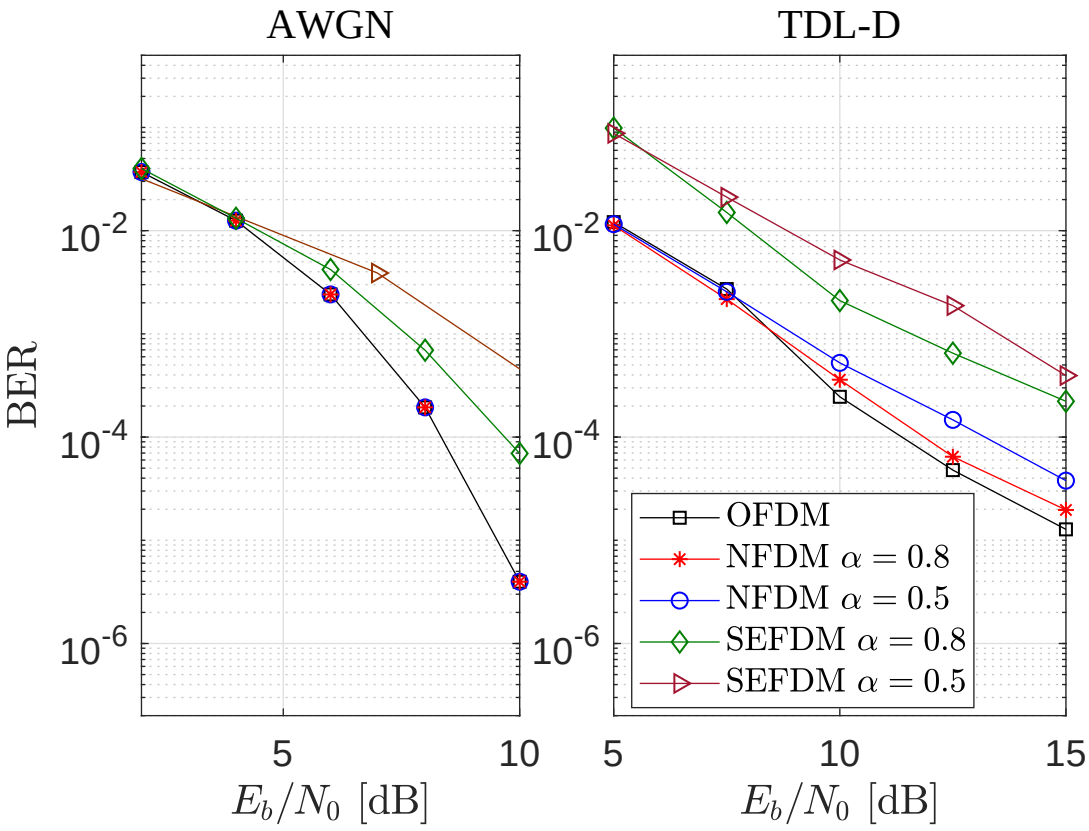

Figure 4.3: Bit error rate performance.

dB. Furthermore, such BER performance of ZP-SEFDM is obtained with a sphere decoder, which is much more complicated that the receiver of the proposed CP-NFDM.

4.5.2 Spectral Efficiency

Given that the proposed CP-NFDM clearly outperforms the state-of-the-art ZP-SEFDM and has lower computational complexity, this section focuses on spectral efficiency comparison between NFDM and OFDM. This quantity is defined as $\eta = \frac{\lambda_b}{T_s B}$, where λ_b is the number of bits per symbol, T_s is the symbol duration, and B is the occupied bandwidth. Of course a spectral efficiency value needs to be interpreted with some reliability measure in mind. A common measure is the bit error rate (BER), which is taken to be 10^{-6} in our comparison. For each system design, such a target BER requires a certain SNR per bit, denoted as $E_b/N_0 = E_s/(\lambda_b N_0)$.

For OFDM, the spectral efficiency can be found as $\eta_1 = \frac{N \log_2(M_1)}{T_s B} \frac{N}{N+L_1}$, where M_1 is the constellation size used in OFDM. Likewise, the spectral efficiency of NFDM can be calculated as $\eta_2 = \frac{N_a \log_2(M_2)}{T_s B'} \frac{N}{N+L_1}$, where N_a is the number of active subcarriers and M_2 is the constellation size.

Fig. 4.4 compares the efficiency of different NFDM systems corresponding to $\alpha \in \{0.1, 0.2, 0.5, 1\}$ at different $\frac{P'}{P}$. Note that OFDM corresponds to $\alpha = 1$. When B' is defined to contain $\frac{P_l}{P} = 98\%$ signal power, one can observe that NFDM with a higher compression factor yields a higher spectral efficiency. For example, OFDM ($\alpha = 1$) requires E_b/N_0 of 15.4 dB to achieve $\eta_1 = 3.9$ bits/s/Hz, while NFDM designed with $\alpha = 0.1$ can achieve $\eta_2 = 4.2$ bits/s/Hz at the same E_b/N_0. A similar performance gain can be seen when higher modulation orders are used. For example, with $\alpha = 0.1$, NFDM is 0.6 bits/s/Hz better than OFDM with 64-QAM.

Similar comparison is also presented in Fig. 4.4 when $\frac{P_l}{P} = 90\%$. One can notice that, once the spectral leakage requirement is loosened, the spectral efficiency of NFDM increases larger than that of OFDM. For instance, OFDM with 16-QAM achieves $\eta_1 = 4$ bits/s/Hz with $E_b/N_0 = 15.4$ dB, while NFDM with $\alpha = 0.1$ attains $\eta_2 = 5.2$ bits/s/Hz. When using higher modulation orders such as $M_1 = M_2 = 64$, the performance gap is even larger, as

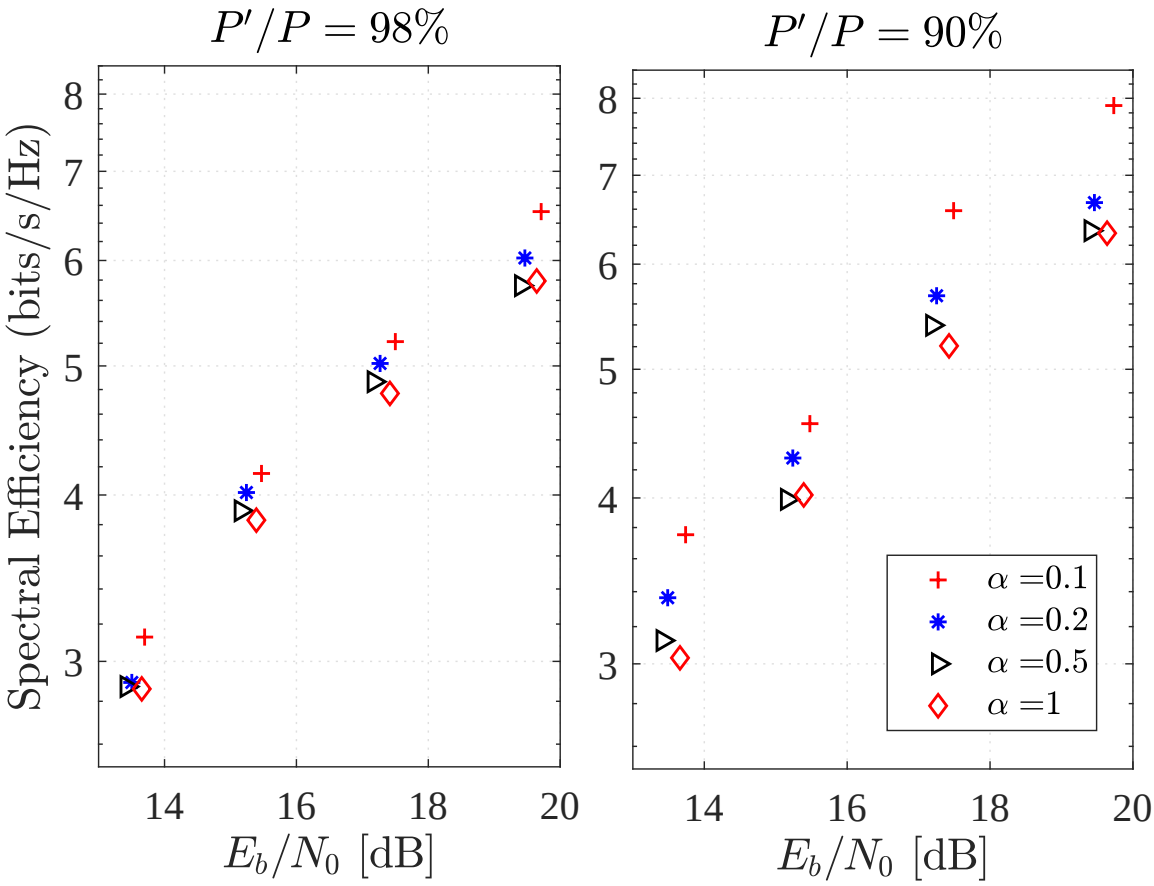

Figure 4.4: Bandwidth-power performance.

$\eta_1 = 6.4$ and $\eta_2 = 7.9$ bits/s/Hz. This corresponds to an approximately 23% improvement in spectral efficiency by using NFDM as compared to OFDM. Overall, the analysis suggests that NFDM designed with $\alpha = 0.1$ provides the best operating points on the bandwidth-power plane provided that the same modulation type and E_b/N_0 are used.

4.6 Conclusion

We proposed a novel NFDM scheme and an associated transceiver design that is immune to ICI, regardless of the bandwidth compression factor. In addition, a novel CP extension was presented, which prevents discontinuities in the transmitted signal and helps to control the power spectrum. Numerical results confirm that this design achieves better bandwidth efficiency than OFDM while meeting a specified target BER, yielding an improvement of up to 23%. Increasing the number of active subchannels and their corresponding scaling factors can impact the transmitted power, peak-to-average power ratio (PAPR), and implementation complexity, so the optimization of these parameters is a promising topic for future study. It is also worthwhile to investigate in detail performance of the proposed SVD-based NFDM when used with the conventional ZP and CP techniques

5. SVD-Based NFDM with Index Modulation

To be submitted as:

Nghia H. Nguyen, Ha H. Nguyen, and Brian Berscheid, "SVD-Based NFDM with Index Modulation".

The previous chapter has provided an innovative design for NFDM systems in which parallel subchannels are realized at the receiver without interference. This chapter incorporates the index modulation technique presented in 3 into the proposed NFDM systems. Specifically, a similar two-stage detection method and its error probability are derived for the resulting NFDM-IM systems. The analysis suggests using modified QAM constellations to achieve the best error performance. Our comprehensive studies on the optimized system suggest that spectral efficiency enhancement is attainable under particular system settings.

SVD-Based NFDM with Index Modulation

Nghia H. Nguyen, Ha H. Nguyen, and Brian Berscheid

Abstract

This paper proposes a novel non-orthogonal frequency division multiplexing (NFDM) with index modulation (NFDM-IM) system for low-rate low-power applications. The system builds on the recently proposed SVD-based NFDM design, which eliminates inter-carrier interference (ICI) in conventional NFDM design. The proposed system enjoys simple two-stage detection and can benefit from using improved signal constellations to improve the system error performance. Results show that the bit error rate (BER) performance of the proposed NFDM-IM approaches that of NFDM while providing a higher transmission rate when low modulation orders are employed. In particular, with the use of an improved 8-QAM constellation, 13% improvement in spectral efficiency is obtained.

5.1 Introduction

Non-orthogonal frequency-division multiplexing (NFDM) is considered as a promising substitute for the conventional orthogonal frequency-division multiplexing (OFDM). The main idea of NFDM is that, by packing subcarriers closer than the minimum spacing required for orthogonality as in OFDM, a smaller bandwidth is consumed while delivering an equal data rate. However, such an advantage is generally challenged by possible performance degradation due to inter-carrier interference (ICI). Such interference becomes more severe as the subcarrier spacing is reduced.

To date, there are a few designs to combat the ICI problem in NFDM. Of course, the best error performance that NFDM[1] can achieve is by employing the maximum likelihood (ML) detector [8]. To avoid the very high (in many cases, impractical) complexity, alternative detection methods have been discussed in [32, 38]. These methods, however, suffer from large performance degradation.

[1]Another common name for NFDM is spectrally-efficient frequency-division multiplexing (SEFDM), which is used in [8].

Instead of examining low-complexity alternatives to the ML receiver, a recent work in [10] revisits the design of both the transmitter and receiver in an NFDM system. With the design proposed in [10], the singular-value decomposition (SVD) of the modified Fourier matrix is performed to obtain precoding and decoding matrices for the transmitter and receiver, respectively, which helps to completely eliminate ICI at the receiver in an AWGN channel. In particular, the design in [10] converts the NFDM system into a set of parallel independent subchannels, i.e., similar to OFDM, albeit with the number of effective channels less than the number of subcarriers. Nevertheless, comparison to OFDM under the same bit error rate performance and transmit power, the design in [10] shows that NFDM can enjoy spectral efficiency enhancement of 23% for certain system configurations. Such spectral efficiency enhancement comes at very little complexity increase when compared to OFDM.

In a different line of research, the concept of index modulation (IM) has been extensively explored to increase the data rate of a conventional OFDM system [39]. In such a system, called OFDM-IM, instead of sending constellation symbols over all subcarriers at any given time, the patterns of activated subcarriers are determined by the so-called index bits. This means that a portion of information bits can be used to index, and hence be carried by, the subcarrier activation patterns. Although a portion of constellation bits are "lost" in those inactive subcarriers (when compared to OFDM), the loss could be well compensated by the amount of index bits. At the receiver, the ML detection can be employed, but only when the employed signal constellation is small and the number of subcarriers is not very large [15,25]. Alternatively, the two-stage detection method discussed in [14] is a more practical choice, which sacrifices some performance degradation for a much simpler implementation.

The applicability of the IM concept is not just limited to OFDM. As a matter of fact, the integration of IM with NFDM has been considered in [40, 41]. It is important to point out that the studies in [40, 41] combine IM with the *conventional NFDM*, and as such, require the use of the highly-complicated ML detection to adequately handle the inherent ICI. This also means that the systems in [40, 41] are limited to the use of small constellations such as BPSK and QPSK for reasons of computational complexity, and therefore are only applicable to the very low spectral efficiency regime.

Given the clear advantages of the SVD-based NFDM design in [10] over the conventional NFDM, it is natural and interesting to combine it with IM. This is precisely the objective of this paper. Thanks to the nonexistence of ICI in the SVD-based NFDM, we can apply the low-complexity two-stage detection method used in conventional OFDM-IM to the proposed NFDM-IM system. This involves detecting the subcarrier pattern first, followed by the demodulation of constellation symbols. By analyzing the potential sources of bit errors in the resulting system, we also design constellations to optimize the system performance. In particular, results show that the proposed NFDM-IM with an improved 8-QAM constellation enjoys 13% improvement compared to SVD-based NFDM in terms of spectral efficiency.

The rest of the paper is organized as follows. Section 5.2 reviews the SVD-based NFDM design in [10] and introduces the NFDM-IM system. The two-stage detection method and its error performance analysis are presented in Section 5.3. Also presented in this section are improved 8-QAM and 16-QAM constellations. Numerical results on error performance and spectral efficiency are provided in Section 5.4. Finally, Section 5.5 concludes the paper.

5.2 System Model

This part reviews the key signal processing steps of the NFDM design proposed in [10]. At the transmitter, most signal processing steps are similar to that in the conventional OFDM transmitter, except the use of a modified Fourier transform. With N subcarriers, this transform is represented by matrix $\mathbf{F}$ where the n,kth element is defined by $f_{n,k} = \frac{1}{\sqrt{N}} \exp\left(j2\pi\alpha nk/N\right)$, $n,k \in \{0,\ldots,N-1\}$ and $\alpha < 1$ is the compression factor. The value of α determines how much the subcarrier spacing in NFDM is compressed as compared to OFDM.

Let $\mathbf{F} = \mathbf{U}\mathbf{D}\mathbf{V}^{\mathrm{H}}$ be the singular value decomposition of $\mathbf{F}$. In SVD-based NFDM design, only $N_a \leq N$ subchannels are active, where N_a is properly chosen to strike a balance between having well-behaved power spectral density and good spectral efficiency. Let $\mathbf{s} = [s_0,\ldots,s_{N_a-1},0,\ldots,0]$ denote a length-N baseband symbol vector. This signal is precoded with matrix $\mathbf{V}$ and scaled by $\mathbf{G} = \mathrm{diag}\{[g_0,\ldots,g_{N-1}]\} = \mathbf{D}^{-1}$. Then, the transmit

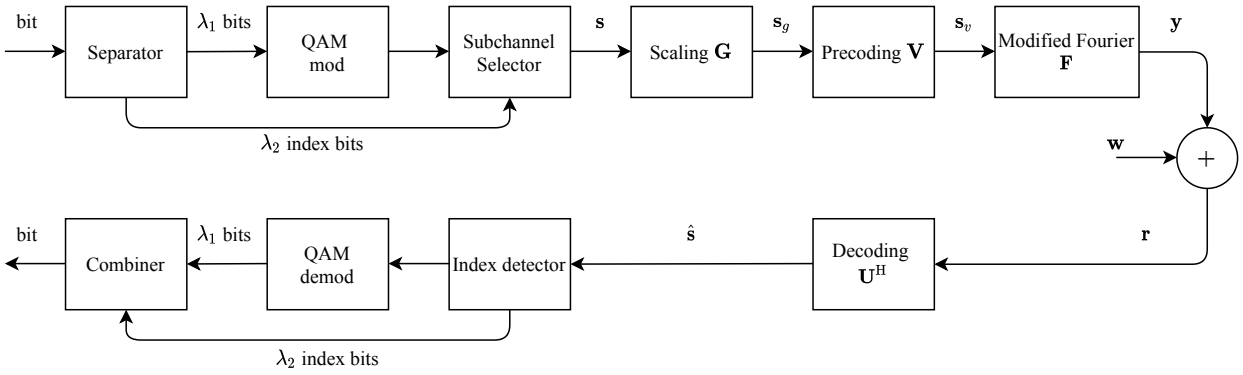

Figure 5.1: Block diagram of the proposed NFDM-IM system.

NFDM signal can be expressed as

$$\mathbf{y} = \mathbf{FVGs} = \mathbf{Us}. \tag{5.1}$$

Over an AWGN channel, the received signal is

$$\mathbf{r} = \mathbf{Us} + \mathbf{w}, \tag{5.2}$$

where $\mathbf{w} \sim \mathcal{CN}(0, N_0\mathbf{I})$. Then, one can apply the transformation $\mathbf{U}^{\mathrm{H}}$ on $\mathbf{r}$ to obtain $\hat{\mathbf{s}} = \mathbf{U}^{\mathrm{H}}\mathbf{r} = \mathbf{s} + \mathbf{U}^{\mathrm{H}}\mathbf{w}$. Since $\mathbf{U}$ is unitary, $\mathbf{U}^{\mathrm{H}}\mathbf{w}$ is also distributed as $\mathcal{CN}(0, N_0\mathbf{I})$. This means that, as far as demodulation of $\hat{\mathbf{s}}$ is concerned, there are N_a parallel subchannels that are independent from each other and have the same SNR. This important property inspires our proposal to combine SVD-based NFDM with index modulation.

Fig. 5.1 shows the block diagram of the proposed combination of NFDM with index modulation, called NFDM-IM. First, λ information bits are separated into λ_1 constellation bits and λ_2 index bits, where $\lambda = \lambda_1 + \lambda_2$. The constellation bits are mapped to constellation symbols, while the index bits determine the set of K out of N_a subchannels, denoted as $\mathcal{K}$, to carry those constellation symbols. Obviously, the number of index bits is $\lambda_2 = \left\lfloor \log_2 \left(\frac{N_a!}{K!(N_a-K)!} \right) \right\rfloor$. The symbol vector $\mathbf{s}$ is $\mathbf{s} = [s_0, \ldots, s_{N_a-1}, 0, \ldots, 0]$, where s_i is an M-QAM symbol if $i \in \mathcal{K}$, and zero otherwise.

The remaining steps in the transmitter are the same as that in the SVD-based NFDM transmitter, and the output signal is given as $\mathbf{y} = \mathbf{Us}$. The average NFDM-IM symbol

energy can be calculated as

$$\mathcal{E}\{||\mathbf{y}||^2\} = \mathcal{E}\left\{||\mathbf{s}||^2\right\} = \left\{\sum_{i\in\mathcal{K}}^{K} \mathcal{E}|s_i|^2\right\} = K\bar{E}, \tag{5.3}$$

where $\bar{E}$ is the average symbol energy of the constellation.

As pointed out above, by applying the transform operation $\mathbf{U}^{\mathrm{H}}$ on $\mathbf{y}$, one obtains the set of N_a parallel subchannels as in (5.2). It follows that, similar to OFDM-IM [14, 42], the detection process can be carried out in two steps: The first step is to detect the set of active subcarriers, denoted as $\hat{\mathcal{K}}$, and the second step is to demodulate λ_1 constellation bits from these subcarriers. Note that this is markedly different from the complicated ML detection required for the conventional NFDM-IM system as in [41]. Specifically, the K active channels are detected as

$$\min\{|\hat{s}_i|^2\} \geq \max\{|\hat{s}_n|^2\}, \quad 1 \leq i \in \mathcal{K}, n \notin \mathcal{K} \leq N_a. \tag{5.4}$$

The index bits are recovered from the detected indexes, whereas the constellation bits are detected from the symbol set $\{\hat{s}_i\}$.

In the next section, performance analysis of the proposed NFDM-IM is discussed and designs of QAM constellations are presented to improve the system's error performance.

5.3 Performance Analysis and Constellation Design

5.3.1 Performance Analysis

Similar to the analysis in [42] for fast OFDM-IM, the overall error event is caused by errors made in one of the two detection stages. In the first stage, an error is made when at least one subchannel in the inactive set is marked as "active". The probability of this event can be calculated as

$$P_{\mathrm{idx}} = P(X_{\min} < Z_{\max}) = \int_0^\infty F_{X_{\min}}(x) f_{Z_{\max}}(x) dx, \tag{5.5}$$

where $X_{\min}$ is the random variable representing the minimum magnitude of the received signals in the K active subchannels, while $Z_{\max}$ is the maximum value in the remaining

$N_a - K$ inactive subchannels. The functions $F_X(\cdot)$ and $f_X(\cdot)$ generally denote the cdf and pdf of random variable X.

Let X and Z be the magnitudes of the received signals corresponding to any active and inactive subchannels, respectively. They can be shown to have the forms $X = |(a + jb) + w|$ and $Z = |0 + w|$, where $(a + jb)$ represents a constellation symbol and $w \sim \mathcal{CN}(0, N_0)$. The cdf of X can be obtained by averaging over M constellation symbols, which is

$$F_X(x) = \frac{1}{M} \sum_{m=1}^{M} 1 - Q_1(\mu_m, x). \tag{5.6}$$

In the above expression $\mu_m = \sqrt{a_m^2 + b_m^2}$ is the Euclidean distance from the mth constellation symbol to the origin, and Q_1 is the Marcum Q-function. On the other hand, Z is Rayleigh distributed, whose pdf and cdf are $F_Z(x) = 1 - \exp(-x^2/N_0)$, and $f_Z(x) = \frac{x}{N_0/2} \exp(-x^2/N_0)$.

Note that

$$F_{X_{\min}}(x) = 1 - (1 - F_X(x))^K, \tag{5.7}$$

$$\begin{aligned} f_{Z_{\max}}(x) &= \frac{dF_{Z_{\max}}(x)}{dx} = \frac{d(F_Z(x))^{N_a - K}}{dx} \\ &= (N_a - K)(F_Z(x))^{N_a - K - 1} f_Z(x). \end{aligned} \tag{5.8}$$

Plugging $F_Z(x)$, $f_Z(x)$ and $F_X(x)$ into (5.5) yields

$$\begin{aligned} P_{\text{idx}} =& (N_a - K) \int_0^\infty \left(1 - (1 - \frac{1}{M} \sum_{m=1}^{M} 1 - Q_1(\mu_m, x))^K \right) \\ & (1 - \exp(-x^2/N_0))^{N_a - K - 1} \frac{x}{N_0/2} \exp(-x^2/N_0) dx, \end{aligned}$$

which can be numerically evaluated.

The overall bit error probability can be expressed as

$$\begin{aligned} P_e =& \underbrace{P_{\text{idx}} \left(\frac{\lambda_2}{2\lambda} + \frac{\lambda_1}{\lambda} \left(\left(\frac{K-2}{K} \right) P_{\text{const}} + \frac{1}{K} \right) \right)}_{P_{e,1}} \\ & + \underbrace{(1 - P_{\text{idx}}) \frac{\lambda_1}{\lambda} P_{\text{const}}}_{P_{e,2}}, \end{aligned} \tag{5.9}$$

where $P_{e,1}$ and $P_{e,2}$ are probabilities of error corresponding to the incorrect and correct index detection events, respectively, whereas P_{const} is the bit error probability of the constellation.

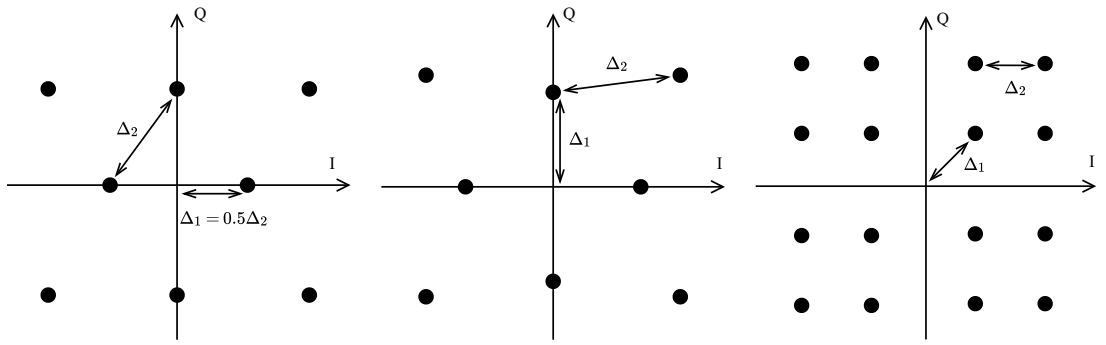

(a) Original hexagonal 8-QAM (b) Improved hexagonal 8-QAM (c) Improved 16-QAM

Figure 5.2: Constellation designs for 8-QAM and 16-QAM.

5.3.2 Constellation Design

With the two-step detection process, errors can be made at either or both steps. One may observe that the likelihood of incorrectly detecting which subcarriers are active is strongly influenced by the minimum distance from the origin to any constellation point (denoted as Δ_1), whereas the error in detecting the constellation bits is largely determined by the minimum distance between constellation points (denoted as Δ_2). As such, it makes sense and is beneficial to properly design a constellation to strike an optimum balance among the two types of errors, leading to a minimum value of P_e. In the context of low-rate communications, we shall focus on the design of small constellations[2] namely 8-QAM and 16-QAM.

Hexagonal 8-QAM

The original hexagonal 8-QAM constellation is shown in Fig. 5.2a, where $\Delta_1 = 0.5\Delta_2$. It is worth noting that this is the best among many 8-ary constellations in terms of error performance [16] when applied in a single-carrier system over an AWGN channel. The exact bit error probability for this constellation is given as [19]

$$P_{\text{const}} = \frac{1}{3}\left(CQ(\Delta_2/(2\sigma)) - C_K C_A\right), \tag{5.10}$$

[2]Due to the perfect symmetry of BPSK and QPSK, there is no flexibility to optimize these two constellations.

where $\sigma = \sqrt{N_0/2}$. The constants $C = 13/4$, $C_K = 9/4$ are the average number of nearest neighbours of all constellation points and the average number of pairs of nearest neighbours, respectively. The coefficient C_A is the correction term to compensate for double counting of the overlap of a 3-PSK constellation and is given by

$$C_A = 2Q\left(\frac{\Delta_2}{2\sigma}\right) Q\left(\frac{\Delta_2}{2\sqrt{3}\sigma}\right) - \frac{2}{3}Q^2\left(\frac{\Delta_2}{\sqrt{6}\sigma}\right). \tag{5.11}$$

Fig. 5.3 shows that there is a significant gap between P_{const} and P_e, which implies that the overall error rate is dominated by the scenario where the active subcarriers are incorrectly detected. This result can intuitively be predicted by the short distance from the origin to its nearest points in the conventional hexagonal 8-QAM system. To improve P_e, an improved 8-QAM constellation is suggested as in Fig. 5.2b. It is designed such that $\Delta_2 \leq \sqrt{2}\Delta_1$, which ensures Δ_2 is the smallest distance.

With the proposed 8-QAM design, the bit error probability of the constellation is given as

$$\begin{aligned} P_{\text{const}} &= \frac{1}{3}\left(\frac{1}{8}\sum_{m=1}^{M} P\{s_{m'\neq m}|s_m\} - B_K B_A\right) \\ &= \frac{1}{3}\Bigg(2Q\left(\frac{\Delta_2}{2\sigma}\right) + Q\left(\frac{\Delta_1}{\sqrt{2}\sigma}\right) \\ &\qquad + 0.5Q\left(\frac{\Delta_1}{\sigma}\right) - B_K B_A\Bigg), \end{aligned} \tag{5.12}$$

where $B_K = C_K$ and

$$B_A \approx 2Q\left(\frac{\Delta_2}{2\sigma}\right) Q\left(\frac{\Delta_2}{2\sqrt{3}\sigma}\right) - \frac{2}{3}Q^2\left(\frac{\Delta_2}{\sqrt{6}\sigma}\right). \tag{5.13}$$

By defining $\beta = \Delta_1/\Delta_2$, the error probability term P_{const} in Eq. (5.9) can be expressed as a function of β and Δ_1 as

$$\begin{aligned} P_{\text{const}} =& \frac{1}{3}\Bigg(2Q\left(\frac{\Delta_2}{2\sigma}\right) + Q\left(\frac{\beta\Delta_2}{\sqrt{2}\sigma}\right) + 0.5Q\left(\frac{\beta\Delta_2}{\sigma}\right) \\ &- \frac{13}{2}Q\left(\frac{\Delta_2}{2\sigma}\right) Q\left(\frac{\Delta_2}{2\sqrt{3}\sigma}\right) - \frac{13}{6}Q^2\left(\frac{\Delta_2}{\sqrt{6}\sigma}\right)\Bigg) \end{aligned} \tag{5.14}$$

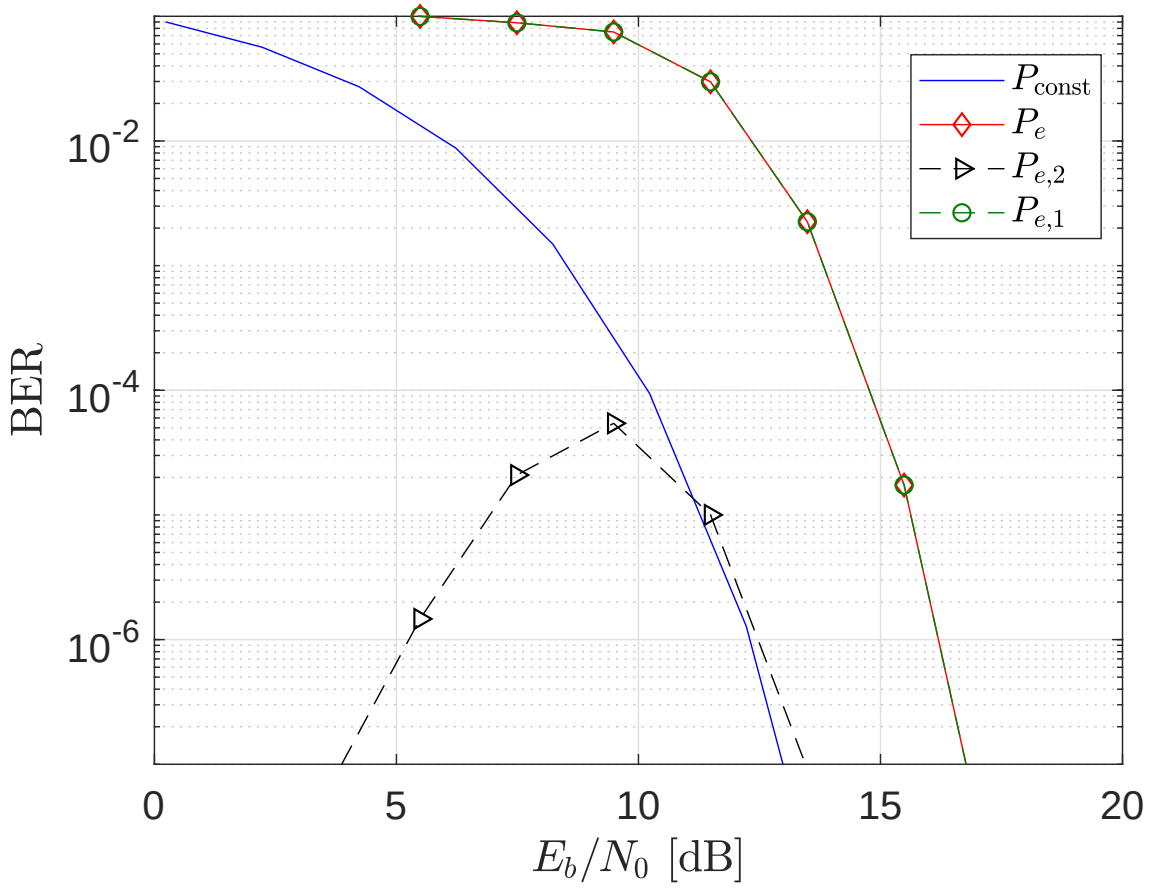

Figure 5.3: Components of the error probability for NFDM-IM with conventional hexagonal 8-QAM.

On the other hand, P_{idx} is calculated from $F_X(x)$, which is

$$\begin{aligned} F_X(x) &= \frac{1}{M}\sum_{m=1}^{M} 1 - Q_1(\mu_m, x) \\ &= 1 - \frac{1}{2}Q_1(\beta\Delta_2, x) - \frac{1}{2}Q_1\left(\frac{\Delta_2\sqrt{(2-\beta^2)}+\beta}{\sqrt{2}}, x\right). \end{aligned} \tag{5.15}$$

Under the average constellation energy constraint $\bar{E} = 0.5(\beta^2 + 1 + \beta\sqrt{2-\beta^2})\Delta_2^2$, the optimal value of β for each $\bar{E}$ can be found by a numerical search in order to minimize P_e.

Rectangular 16-QAM

The improved rectangular 16-QAM constellation is shown in Fig. 5.2c. The bit error probability of such a constellation can be calculated as

$$P_{\text{const}} = \frac{1-(1-P_{\text{const-1D}})^2}{\log_2 M}, \tag{5.16}$$

where $P_{\text{const-1D}}$ is the symbol error probability of the corresponding one dimensional 4-ASK constellation. This error probability can be shown to be

$$P_{\text{const-1D}} = Q\left(\frac{\Delta_2}{2\sqrt{N_0/2}}\right) + \frac{2}{\sqrt{M}}Q\left(\frac{\beta\Delta_2}{\sqrt{N_0}}\right). \tag{5.17}$$

Under the average symbol energy constraint of $\bar{E}$, Δ_2 and β are related by

$$\Delta_2 = \frac{\bar{E}}{\beta^2 + \beta\sqrt{2} + 1} \tag{5.18}$$

Furthermore, the adjustment of the symbol locations in the signal space changes the distribution of X to

$$\begin{aligned} F_X(x) &= \frac{1}{M}\sum_{m=1}^{M} 1 - Q_1(\mu_m, x) \\ &= 1 - \frac{1}{4}\Big[Q_1(\mu_1, x) + Q_1(\mu_2, x) \\ &\qquad + Q_1(\mu_3, x) + Q_1(\mu_4, x)\Big], \end{aligned} \tag{5.19}$$

where

$$\mu_1 = \Delta_1 = \beta\Delta_2, \tag{5.20}$$

$$\mu_2 = \mu_3 = \Delta_2\sqrt{\frac{3}{2}\beta^2 + \beta\sqrt{2} + 1}, \tag{5.21}$$

$$\mu_4 = \Delta_2\sqrt{\beta^2 + 2\sqrt{2}\beta + 2}. \tag{5.22}$$

Again, numerical search is sufficient and simple enough to find the optimal ratio β to achieve the best error performance.

5.4 Numerical Results

In this section, numerical results for the proposed NFDM-IM with improved constellations are presented. The number of subcarriers is $N = 128$, the compression factor $\alpha \in \{1, 0.5, 0.2\}$, and the subcarrier spacing is $\Delta_f = 15$ kHz. The number of active subcarriers N_a is determined based on a heuristic rule: $g_i \leq 1$ with $i \in \{1, \ldots, N_a\}$ (see in [10] and [43] for justification). With N_a being the total number of subchannels available for indexing, the optimal number of subchannels that should be activated in a given symbol duration should be $K = \frac{M}{M+1}N_a$ in order to maximize the spectral efficiency [42], which is $\eta = \frac{\lambda}{T_s B}$, where $T_s = 1/\Delta_f$ is the symbol duration. Another important factor is the occupied bandwidth, which is approximated as $B \approx \alpha(N-1)\Delta_f + \Delta_f$.

Table 5.1 presents the comparison between SVD-based NFDM in [10] and the NFDM-IM (with the improved constellation) proposed in this paper when $M = 8$. One can see that, with $\alpha = 0.2$, the highest bandwidth efficiency of 3.48 bits/s/Hz is achieved by the proposed NFDM-IM, while NFDM without index modulation yields 3.06 bits/s/Hz. However, when $M = 16$, the results presented in Table 5.2 show that, even by using the improved 16-QAM constellation, there is no benefit in spectral efficiency by exploiting index modulation. This is because with a higher constellation such as 16-QAM, the amount of index bits is not high enough to compensate for the reduction in constellation bits due to inactive subchannels in NFDM-IM.

Next, comparison of the bit error probabilities is made for the following three SVD-

Table 5.1: Comparison when $N = 128,\ M = 8$.

	α	N_a	K	B (kHz)	λ	η (bits/s/Hz)
NFDM	1	128	n/a	1920	384	3.0
	0.5	64	n/a	967	192	2.97
	0.2	27	n/a	396	81	3.06
NFDM-IM	1	128	113	1920	384	3.14
	0.5	64	56	967	200	3.1
	0.2	27	24	396	92	3.48

Table 5.2: Comparison when $N = 128,\ M = 16$.

	α	N_a	K	B (kHz)	λ	η (bits/s/Hz)
NFDM	1	128	n/a	1920	512	4
	0.5	64	n/a	967	256	3.96
	0.2	27	n/a	396	108	4.1
NFDM-IM	1	128	113	1920	515	4.02
	0.5	64	56	967	256	3.96
	0.2	27	24	396	107	4.05

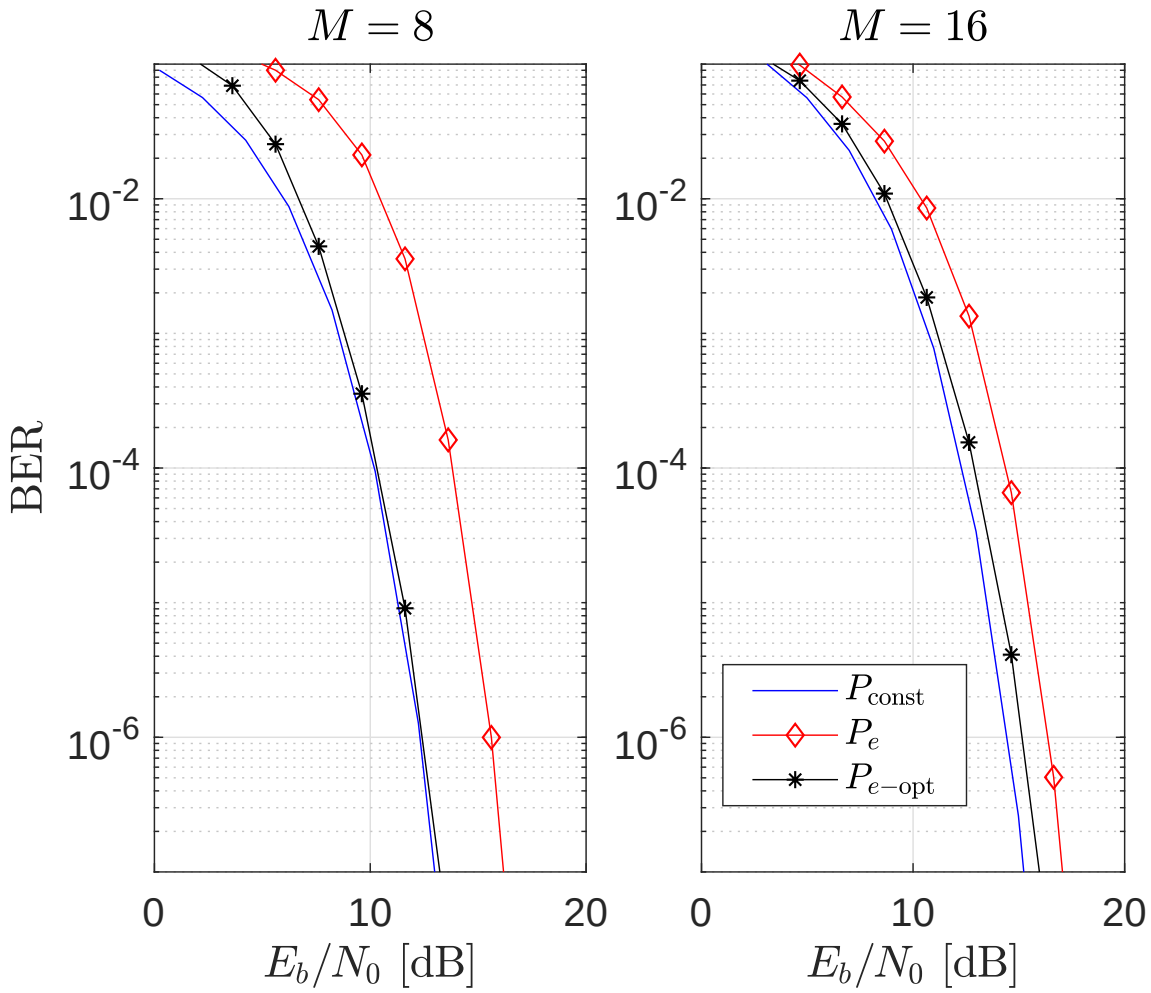

Figure 5.4: BER comparison.

based systems: NFDM (P_{const}), NFDM-IM with conventional constellation (P_e) and NFDM-IM with the improved constellation ($P_{e-\text{opt}}$). For the results presented in Fig. 5.4, the compression factor is $\alpha = 0.2$. It can be observed that when $M = 8$, to obtain a BER of 10^{-6}, NFDM-IM with the regular 8-QAM requires $E_b/N_0 = 15.5$ dB, while NFDM-IM with the improved 8-QAM needs only 12.2 dB, i.e., there is 3.3 dB gain. In comparison with SVD-based NFDM, the NFDM-IM with improved 8-QAM basically achieves the same error rate, especially when $E_b/N_0 > 10$ dB. While having the same error performance, NFDM-IM with the improved constellation enjoy a 13% enhancement in spectral efficiency, specifically at 3.48 bits/s/Hz as compared to 3 bits/s/Hz of the SVD-based NFDM.

When $M = 16$, one can also observe a 1.1 dB gain when the improved constellation is used in NFDM-IM instead of the regular 16-QAM constellation (i.e., by comparing P_e and $P_{e-\text{opt}}$). However, there is still a gap of 0.2 dB for NFDM-IM with improved 16-QAM to match the performance of the SVD-based NFDM. Since both the error performance and spectral efficiency of NFDM-IM are not better than SVD-based NFDM for $M = 16$, it is likely that there is no benefit in designing large constellations ($M \geq 16$) for NFDM-IM.

5.5 Conclusion

In this paper, the combination of SVD-based NFDM and index modulation was proposed and analyzed. The ICI that exists in the conventional NFDM is eliminated with SVD-based NFDM design, which allows simple signal detection when combined with index modulation. Furthermore, signal constellations are designed to improve the overall system error performance. Results show that at the target BER of 10^{-6}, a 13% enhancement in spectral efficiency can be obtained over SVD-based NFDM by using the proposed NFDM-IM with the improved 8-QAM constellation. In general, the application of index modulation to the frequency dimension in a multi-carrier system, whether it is OFDM or SVD-based NFDM, is only beneficial in low-rate low-power scenarios.

6. Summary

6.1 Summary

This thesis has focused on improving spectral efficiency for multicarrier systems in the context of IoT applications. Generally, there are two approaches to accomplish this goal, namely increasing data rate and reducing occupied bandwidth.

One approach to increasing data rate is the use of index modulation in conjunction with fast-OFDM. As investigated in Chapter 3, the combination of fast-OFDM with index modulation and one-dimension constellations produces significant improvements in terms of bit rate compared to the conventional OFDM, especially when low modulation orders are employed, as in the case of IoT. The bit error probability using a practical detection method is also derived for this system, which suggests an optimal constellation choice to improve the performance. Obtained results confirm the spectral efficiency enhancements in the proposed system compared to the conventional OFDM system at low modulation orders.

The second approach, reducing occupied bandwidth, can be realized by using a non-orthogonal multicarrier system, i.e., NFDM. The occupied bandwidth in NFDM is typically less than that of OFDM thanks to a smaller subcarrier spacing, however it comes with severe error performance degradation in the conventional transceiver design. Inspired by this fact, Chapter 4 proposed a novel design for NFDM systems, which is capable of eliminating inter-carrier interference and providing an identical error performance as in OFDM systems over AWGN channels. The spectrum of its transmit signal was studied, showing its limitation and motivating the use of a proper spectrum control method. The use of such a method yields smaller bandwidths, helping NFDM systems achieve higher spectral efficiency than

that of OFDM systems.

Finally, both approaches to improve spectral efficiency are combined in Chapter 5, where the index modulation approach in Chapter 3 is applied to the new NFDM design from Chapter 4. Constellation optimization similar to that studied in Chapter 3 was performed in the proposed system, resulting in an equivalent error performance as in the conventional OFDM and NFDM. In terms of spectral efficiency, an improved operating point was found by using the proposed scheme, consisting of NFDM-IM with an optimized 8-QAM constellation. This scheme is well-suited to the low-power low-rate requirements of IoT applications.

6.2 Future Studies

There are a number of opportunities to build upon the results presented in this thesis through future studies.

- Unlike OFDM systems, the spectrum shape of transmit signals in NFDM systems is dependent on the number of active channels which carry QAM symbols. Thorough experiments show that for NFDM systems to achieve a similar level of out-of-band (OOB) power radiation as in OFDM systems, the number of active channels varies approximately proportionally to the compression factor, limiting true bit rate of the NFDM system. Alternative methods of activating, scaling and shaping the subcarriers to balance the OOB radiation and the data rate could yield further improvements.

- The proposed SVD-based NFDM systems in Chapter 4 encourage the use of the continuous cyclic prefix extension method to combat with multipath channels. While it is particularly helpful in suppressing the OOB radiation in the PSD, obtained error performance over multipath channels was not as good as the one with conventional cyclic prefix, especially when subcarrier spacing is further reduced. In addition to that, due to the unavailability of single-tap equalizer, expensive equalizers are required to inverse the effect of multipath channels, leading to a hardware-inefficient receiver. Further research in other suitable spectrum control techniques, while retaining simple and effective channel equalizers at the same time, could complete the SVD-based

NFDM system and promote its use in the future.

- Index modulation introduces a new dimension (so-called index dimension) as a means to convey more binary data in one OFDM (or NFDM) symbol. Although an optimal balance between index bits and constellation bits can be obtained, there are subcarriers that carry no information (inactive channels), which is not efficient in bandwidth usage. Given such a situation, one possible alteration is to apply a different constellation to certain subcarriers, rather than inactivating them altogether. This technique, often called dual-mode index modulation, or multi-mode index modulation, may provide potential bit rate enhancement to NFDM systems.

References

[1] M. R. Palattella, M. Dohler, A. Grieco, G. Rizzo, J. Torsner, T. Engel, and L. Ladid, "Internet of Things in the 5G Era: Enablers, Architecture, and Business Models," *IEEE Journal on Selected Areas in Communications*, vol. 34, pp. 510–527, Mar. 2016.

[2] L. Chettri and R. Bera, "A Comprehensive Survey on Internet of Things (IoT) toward 5G Wireless Systems," *IEEE Internet of Things Journal*, vol. 7, pp. 16–32, Jan. 2020.

[3] P. Yadav and S. Vishwakarma, "Application of Internet of Things and Big Data towards a Smart City," in *Proc. IEEE 3rd International Conference On Internet of Things: Smart Innovation and Usages (IoT-SIU)*, pp. 1–5, Feb. 2018.

[4] N. Wang, P. Wang, A. Alipour-Fanid, L. Jiao, and K. Zeng, "Physical-Layer Security of 5G Wireless Networks for IoT: Challenges and Opportunities," *IEEE Internet of Things Journal*, vol. 6, pp. 8169–8181, Oct. 2019.

[5] Y.-P. E. Wang, X. Lin, A. Adhikary, A. Grovlen, Y. Sui, Y. Blankenship, J. Bergman, and H. S. Razaghi, "A Primer on 3GPP Narrowband Internet of Things," *IEEE Communications Magazine*, vol. 55, pp. 117–123, Mar. 2017.

[6] "IEEE Standard for Telecommunications and Information Exchange Between Systems - LAN/MAN Specific Requirements - Part 11: Wireless Medium Access Control (MAC) and Physical Layer (PHY) Specifications: High Speed Physical Layer in the 5 GHz Band," *IEEE Std 802.11a-1999*, pp. 1–102, 1999.

[7] 3GPP, "Release 8," tech. rep., 3GPP, 2008.

[8] I. Darwazeh, H. Ghannam, and T. Xu, "The First 15 Years of SEFDM: A Brief Survey," in *Proc. IEEE 11th International Symposium on Communication Systems, Networks and Digital Signal Processing (CSNDSP)*, pp. 1–7, July 2018.

[9] S. Isam and I. Darwazeh, "Characterizing the Intercarrier Interference of Non-orthogonal Spectrally Efficient FDM System," in *Proc. Networks Digital Signal Processing (CSNDSP) 2012 8th Int. Symp. Communication Systems*, pp. 1–5, July 2012.

[10] N. H. Nguyen, B. Berscheid, and H. H. Nguyen, "SVD-Based Design for Non-Orthogonal Frequency Division Multiplexing," *IEEE Communication Letters*, Dec. 2020. Accepted.

[11] S. Gorbunov and A. Rashich, "Spatial Receive Diversity for SEFDM Based Systems," in *Proc. IEEE 42nd International Conference on Telecommunications and Signal Processing (TSP)*, July 2019.

[12] B. Yu, H. Zhang, X. Hong, C. Guo, A. P. T. Lau, C. Lu, and X. Dai, "Channel Equalisation and Data Detection for SEFDM Over Frequency Selective Fading Channels," *IET Communications*, vol. 12, pp. 2315 – 2323, Nov. 2018.

[13] S. Osaki, M. Nakao, T. Ishihara, and S. Sugiura, "Differentially Modulated Spectrally Efficient Frequency-Division Multiplexing," *IEEE Signal Processing Letters*, vol. 26, pp. 1046–1050, July 2019.

[14] P. K. Frenger and N. A. B. Svensson, "Parallel Combinatory OFDM Signaling," *IEEE Transactions on Communications*, vol. 47, pp. 558–567, Apr. 1999.

[15] R. Abu-alhiga and H. Haas, "Subcarrier-index Modulation OFDM," in *Proc. IEEE 20th International Symposium on Personal, Indoor and Mobile Radio Communications*, pp. 177–181, Sept. 2009.

[16] H. Nguyen and E. Shwedyk, *A First Course in Digital Communications*. Cambridge University Press, 2009.

[17] D. Tse and P. Viswanath, *Fundamentals of Wireless Communication*. Cambridge University Press, 2012.

[18] A. Goldsmith, *Wireless Communications*. Cambridge University Press, 2005.

[19] L. Rugini, "Symbol Error Probability of Hexagonal QAM," *IEEE Communications Letters*, vol. 20, pp. 1523–1526, Aug. 2016.

[20] E. Başar, U. Aygölü, E. Panayrc, and H. V. Poor, "Orthogonal Frequency Division Multiplexing with Index Modulation," *IEEE Transactions on Signal Processing*, vol. 61, pp. 5536–5549, Nov. 2013.

[21] 3GPP, "3GPP Release 14," tech. rep., 3GPP, 2017.

[22] R. Ratasuk, J. Tan, N. Mangalvedhe, M. H. Ng, and A. Ghosh, "Analysis of NB-IoT Deployment in LTE Guard-Band," in *Proc. IEEE 85th Vehicular Technology Conf. (VTC Spring)*, pp. 1–5, June 2017.

[23] B. Yang, L. Zhang, D. Qiao, G. Zhao, and M. A. Imran, "Narrowband Internet of Things (NB-IoT) and LTE Systems Co-existence Analysis," in *Proc. IEEE Global Communications Conf. (GLOBECOM)*, pp. 1–6, Dec. 2018.

[24] S. Oh and J. Shin, "An Efficient Small Data Transmission Scheme in the 3GPP NB-IoT System," *IEEE Communications Letters*, vol. 21, pp. 660–663, March 2017.

[25] Y. Ko, "A Tight Upper Bound on Bit Error Rate of Joint OFDM and Multi-Carrier Index Keying," *IEEE Communications Letters*, vol. 18, pp. 1763–1766, Oct. 2014.

[26] G. Sheng, S. Dang, Z. Zhang, E. Kocan, and M. Pejanovic-Djurisic, "OFDM with Index Modulation Assisted by Multiple Amplify-and-Forward Relays," *IEEE Wireless Communications Letters*, vol. 8, pp. 789 – 792, June 2019.

[27] M. Rodrigues and I. Darwazeh, "Fast OFDM: A Proposal for Doubling the Data Rate of OFDM Schemes," in *Proc. IEEE International Conference on Telecommunications*, pp. 484 – 487, June 2002.

[28] T. Xu and I. Darwazeh, "Non-Orthogonal Narrowband Internet of Things: A Design for Saving Bandwidth and Doubling the Number of Connected Devices," *IEEE Internet of Things Journal*, vol. 5, pp. 2120–2129, June 2018.

[29] A. Papoulis, *Probability, Random Variables, and Stochastic Processes*. McGraw-Hill, 3rd ed., 1991.

[30] T. Xu and I. Darwazeh, "Spectrally Efficient FDM: Spectrum Saving Technique for 5G?," in *Proc. 1st Int. Conf. 5G for Ubiquitous Connectivity*, pp. 273–278, Nov. 2014.

[31] W. Ozan, P. A. Haigh, B. Tan, and I. Darwazeh, "Time Precoding Enabled Non-Orthogonal Frequency Division Multiplexing," in *Proc. IEEE 30th International Symposium on Personal, Indoor and Mobile Radio Communications (PIMRC)*, pp. 1–6, Sept. 2019.

[32] S. Isam, I. Kanaras, and I. Darwazeh, "A Truncated SVD Approach for Fixed Complexity Spectrally Efficient FDM Receivers," in *Proc. IEEE Wireless Communications and Networking Conference*, pp. 1584–1589, Mar. 2011.

[33] M. Jia, Z. Wu, Z. Yin, Q. Guo, and X. Gu, "Receiver Design Combining Iteration Detection and ICI Compensation for SEFDM," *EURASIP Journal on Wireless Communications and Networking*, Feb. 2018.

[34] T. Xu, C. Masouros, and I. Darwazeh, "Waveform and Space Precoding for Next Generation Downlink Narrowband IoT," *IEEE Internet of Things Journal*, vol. 6, pp. 5097–5107, June 2019.

[35] W. Ozan, R. Grammenos, and I. Darwazeh, "Zero Padding or Cyclic Prefix: Evaluation for Non-Orthogonal Signals," *IEEE Communications Letters*, vol. 24, pp. 690–694, Mar. 2020.

[36] X. Zhang, M. Jia, L. Chen, J. Ma, and J. Qiu, "Filtered-OFDM-enabler for Flexible Waveform in the 5th Generation Cellular Networks," in *Proc. IEEE Global Communications Conference (GLOBECOM)*, pp. 1–6, Dec. 2015.

[37] F. Schaich and T. Wild, "Waveform Contenders for 5GOFDM vs. FBMC vs. UFMC," in *Proc. IEEE 6th International Symposium on Communications, Control and Signal Processing (ISCCSP)*, pp. 457–460, May 2014.

[38] T. Xu, R. C. Grammenos, F. Marvasti, and I. Darwazeh, "An Improved Fixed Sphere Decoder Employing Soft Decision for the Detection of Non-orthogonal Signals," *IEEE Communications Letters*, vol. 17, pp. 1964–1967, Oct. 2013.

[39] N. Ishikawa, S. Sugiura, and L. Hanzo, "Subcarrier-Index Modulation Aided OFDM -Will It Work?," *IEEE Access*, vol. 4, pp. 2580 – 2593, May 2016.

[40] H. Liu, L. Liu, and P. Wang, "Spectrally Efficient Nonorthogonal Frequency Division Multiplexing with Index Modulation," in *Proc. IEEE 17th International Conference on Parallel and Distributed Computing, Applications and Technologies (PDCAT)*, pp. 290–293, Dec. 2016.

[41] M. Nakao and S. Sugiura, "Spectrally Efficient Frequency Division Multiplexing With Index-Modulated Non-Orthogonal Subcarriers," *IEEE Wireless Communications Letters*, vol. 8, pp. 233–236, Feb. 2019.

[42] N. H. Nguyen, B. Berscheid, and H. H. Nguyen, "Fast-OFDM with Index Modulation for NB-IoT," *IEEE Communications Letters*, vol. 23, pp. 1157–1160, July 2019.

[43] M. Ganji, X. Zou, and H. Jafarkhani, "A Block-Based Non-Orthogonal Multicarrier Scheme," in *Proc. IEEE Global Communications Conference (GLOBECOM)*, pp. 1–6, Dec. 2019.